NASA CONTRACTOR REPORT

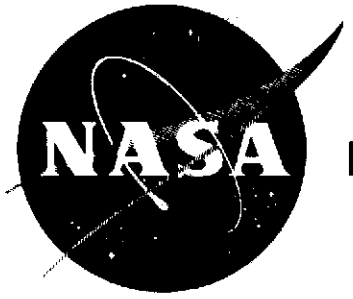


NASA CR-137513

# MICROSTRIP ANTENNA STUDY FOR PIONEER SATURN/URANUS ATMOSPHERE ENTRY PROBE

*by E. A. Kuhlman*



*Prepared by*

MCDONNELL DOUGLAS ASTRONAUTICS COMPANY – EAST
St. Louis, Missouri 63166 (314) 232-0232

*for Ames Research Center*



NATIONAL AERONAUTICS AND SPACE ADMINISTRATION • WASHINGTON, D. C. • MAY 1974

NASA CR-137513

# MICROSTRIP ANTENNA STUDY FOR PIONEER SATURN/URANUS ATMOSPHERE ENTRY PROBE

*by E. A. Kuhlman*



Prepared Under Contract No. NAS 2-7328

by

MCDONNELL DOUGLAS ASTRONAUTICS COMPANY-EAST
Saint Louis, Missouri

for

AMES RESEARCH CENTER

NATIONAL AERONAUTICS AND SPACE ADMINISTRATION

TABLE OF CONTENTS

TABLE OF CONTENTS
(CONTINUED)



LIST OF PAGES

LIST OF FIGURES

LIST OF FIGURES
(CONTINUED)

LIST OF TABLES

# MICROSTRIP ANTENNA STUDY FOR PIONEER SATURN/URANUS ATMOSPHERIC ENTRY PROBE

## SUMMARY

The design parameters of a microstrip antenna were studied to determine its performance characteristics as affected by an atmospheric entry probe environment. The technical literature was reviewed to identify the known design and performance characteristics. These data were used to evaluate the expected effects of mission environments on the microstrip antenna design proposed under Contract NAS 2-7328 for the Saturn/Uranus Atmospheric Entry Probe (SAEP). Radiation patterns and VSWR measurements were made to evaluate the performance in the SAEP thermal environment.

Results of the literature search and pattern tests confirm that the microstrip antenna is a good choice as a transmitting antenna on the SAEP. The microstrip antenna is efficient, compact, and well suited to a space environment. Precise design parameters have not yet been given in the literature and thus some antenna design and test are still necessary. The pattern can be controlled with a minimum beamwidth of 60 degrees (air substrate; e.g., honeycomb structure) and a maximum on the order of 100 degrees with higher dielectric constant substrates. The power handling capacity is good and can be improved by covering the antenna with a dielectric cover.

Temperature and high energy radiation appear to be the primary environmental factors which affect the resonant frequency of the microstrip antenna. The calculated effect was 0.57 MHz increase in resonant frequency due to temperature and a maximum of 2.7 MHz for gamma radiation.

The temperature test results show that the shift in resonant frequency of the microstrip antenna was 1.15 MHz, about twice that calculated. The pattern shape remains essentially constant and the axial ratio increases. The increase in axial ratio is reasonably small with the net loss in circular polarization gain being only 0.5 dB. These tests were run with 2.54 cm (1.0 in.) thick layer of insulation as a dielectric cover and shows the insulation cover has no significant effect on the microstrip antenna performance.

# INTRODUCTION

The objective of this study is to define and evaluate the performance characteristics of the microstrip antenna proposed for the SAEP telecommunication transmitting antenna. The study approach consisted of: (1) analyzing the principle performance parameters to determine the effects of the outer planet environments, and (2) testing the electrical performance of a microstrip antenna at elevated temperature. This is an extension of Contract NAS 2-7328.

The microstrip antenna is a relatively new device, which appeared in the literature only recently. It is characterized by a low profile and a radiation pattern akin to an open-end waveguide. The input impedance is relatively high and normally requires some form of impedance transformation. The microstrip antenna is not a broadband device but has sufficient bandwidth for many spacecraft and missile applications.

This report covers the available literature, and in some cases, material yet unpublished which was obtained in discussions with the respective authors. Test results for the microstrip antenna with an insulating cover are also considered to further evaluate the environmental effects on the antenna performance. The test results are compared with predictions based on information found in the literature.

## DESIGN CONSIDERATIONS

This section discusses the design consideration and general characteristics of the microstrip antenna.

### General

The microstrip antenna is basically a metallic panel patch which is supported parallel to a ground plane by a layer of dielectric material. In practice, such a physical relationship can readily be obtained by the use of a double clad (i.e., metalized on both sides) circuit board commonally used for printed circuit fabrication. The metal on one side of the dielectric substrate serves as a ground plane. The metal on the other side of the substrate is etched away so as to leave a patch of metal and the necessary feed transmission line. A sketch of a rectangular microstrip antenna is shown in Figure 1. The length of the radiating patch antenna is approximately one-half wavelength in the dielectric substrate. The width of the patch is usually about one-half wavelength in free space but may vary from this for particular applications. The thickness may vary from 0.079 to 1.27 cm (1/32 to 1/2 in.) or more depending on the operating frequency, bandwidth, and efficiency requirements.

### Characteristics

This section discusses the various characteristics and parameters associated with the microstrip antenna. The material presented is based on the information given in References 1 through 5 and private communication, P.C., with the authors J. Q. Howell and R. E. Munson, and C. M. Kaloi.

Shape - The microstrip antenna radiating patch (element) may be rectangular, square, circular and probably elliptical. The use of these shapes leads to characteristics such as dual frequency, dual polarization and circular polarization. For example, the rectangular elements can be utilized as a dual frequency antenna with orthogonal polarization at each frequency. A square or circular

element can be fed to obtain orthogonal polarizations at the same frequency or circular polarization. The literature does not show the particular advantages of a circular or square microstrip antenna. However, for a particular application, the form factor of one or the other may be of significant advantage for implementation (e.g., the circular shape of the SAEP ideally accommodates a circular microstrip antenna). It also appears that the circular element has a more symmetrical circular polarization, CP, pattern beam than a square element.

Size - The basic size relationship of the microstrip antenna is illustrated in Figure 1. The length, L, which is parallel to the input feed transmission line is one-half wavelength, $\lambda\varepsilon/2$, as modified by the dielectric constant. The nominal width, W, is approximately one-half wavelength in free space, but it may vary around that value depending on the application. The thickness, t, of the substrate or the distance between the radiating patch and the ground plane is small ($t << \lambda$) compared to a wavelength in order to maintain a low profile low weight device. Thicknesses of 0.079 cm (1/32 in.) and up have been used over a wide frequency range. The literature did not indicate an upper practical thickness limit since one of the principal advantages of the microstrip antenna is its low profile. However, this limit is probably established by the onset of higher order modes in either the radiating patch or the feed transmission line or both, or the input impedance characteristics.

The primary factor other than the wavelength at the operating frequency which determines the size of the antenna is the dielectric constant of the substrate. The dielectric constant, $\varepsilon_r$, reduces the characteristic length by the factor $1/\sqrt{\varepsilon_r}$. To the first order, the length (L) of a microstrip antenna is

$$L = \frac{\lambda}{2} \frac{1}{\sqrt{\varepsilon_r}} \tag{1}$$

where $\lambda$ is the free space wavelength and $\varepsilon_r$ is the substrate dielectric constant. Additional information from Kaloi (P.C.) (Figure 2) indicates that in the frequency range considered (370 to 420 MHz) both the dielectric thickness and dielectric constant have second order effects which reduce the characteristic microstrip element below that calculated by equation (1). The square

microstrip element was assumed in arriving at the data in Figure 2. A reduction in the microstrip element length below that calculated by equation (1) is also apparent when considering the reactance of a small inductance associated with the radiation resistance of the radiating slots shown in Figure 1 (also see Figure 3 in Reference 1). The microstrip element length must be slightly less than $\lambda_\varepsilon/2$ in order to just cancel the reactive component and achieve resonance. Since the reactive component of the slot impedance is a function of the width, the amount of compensation will vary with substrate thickness. Munson estimates the actual microstrip element length to be about $0.48\lambda_\varepsilon$ to $0.49\lambda_\varepsilon$.

For a circular element, the expression relating size to frequency for the lowest order resonance is

$$a = 1.84 \left(\frac{\lambda}{2\pi}\right) \frac{1}{\sqrt{\varepsilon_r}} \qquad (2)$$

where a is the radius of the circular element. Appendix I gives a table of design and measured resonant frequencies for several antennas covering frequencies of UHF to C-band.

An array of microstrip antenna elements can be obtained with a single strip where the strip is fed with a corporate feed system as shown in Figure 3. In order to excite only the TEM (transverse electric magnetic) mode, the number of feed points required is greater than the number of wavelengths of the strip and is equal to 2, 4, 8, 16, 32, etc. For example, if the length of the microstrip radiator is 11 $\lambda_\varepsilon$, the number of feeds must be 16. This requirement is due to the requirements for binary power division and maintaining uniform phase distribution. This configuration gives a broadside radiation pattern where the beamwidth is dependent on the microstrip length. If this strip is wrapped around a cylindrical vehicle, such as a missile or spacecraft, only patterns free of nulls in the roll pattern ($TM_{om}$ free space modes) will be excited. The excitation of higher order modes would result in nulls in the roll pattern. From the literature, it is not clear whether or not a continuous strip could be used successfully in a planar configuration with other than a uniform amplitude and phase distribution, even though the number of feeds exceeds the number of wavelengths ($W/\lambda_\varepsilon$) by one, for the purposes of pointing the beam off broadside.

This can be accomplished, however, by cutting the strip into discrete microstrip elements.

The ground plane must be somewhat larger than the microstrip radiating element to eliminate back radiation and form a unidirection pattern typical of the microstrip antenna. Ground plane extensions of $\lambda/20$ to $\lambda/10$ beyond the radiating element are sufficient (Munson, P.C.). When the mounting surface forms a larger ground plane around a microstrip antenna, the ground plane extension on the substrate is governed by requirements for feed circuitry and mounting screws.

Materials and Construction - In practice, double clad circuit board provides an attractive composite for obtaining the physical relationships required to implement a microstrip antenna. Typical examples are 3M Cu Clad K-6098 or Rogers Corporation RT/duroid 5870 (or 5880). The substrate is a Teflon filled fiberglass laminate which has a dielectric constant of 2.4 to 2.5 and is clad with copper on both sides. The copper on one side of the dielectric substrate serves as a ground plane and would be mounted against a particular mounting surface. The copper on the opposite side is etched away so as to form a radiating patch, the feed microstrip transmission line or auxiliary transmission line components for impedance matching, phasing, or power division purposes. Figure 4 shows a circular microstrip antenna designed for application to the SAEP. This antenna was constructed from 0.318 cm (1/8 in.) 3M Cu Clad K-6098 circuit board.

The microstrip antenna may also be constructed from other materials which can be bonded or otherwise held together in the proper physical relationship. Test antennas have been constructed by NASA-LaRC using aluminum oxide ($\varepsilon_r$ = 8.5) and plexiglass ($\varepsilon_r$ = 2.7) as the dielectric substrate. Some foam, controlled dielectric constant composites, and honeycomb structures could also be used. The metallic ground plane, radiating element, and transmission line could be thin sheet metal (e.g., foil), bonded to the substrate, or a deposited metal. The particular materials selected depend on the environmental and mechanical requirements as well as the electrical requirements.

Feed System - There are two principle methods for feeding a microstrip antenna. The first is shown in Figure 1. Here the feed is a section of

microstrip transmission line. In this method, the transmission is "printed" on the same side of the substrate as the radiating element. The width of transmission line determines the characteristic impedance of the transmission line. The transmission line can be run parallel to the radiating element a short distance from the element without affecting the pattern. The spacing requirements are not reported in the literature. Since the input impedance of the microstrip antenna is about 120 ohms, compared to the 50 ohm cable normally connecting the antenna to a transmitter or receiver, the feed transmission line width can be appropriately tapered or dimensioned to form one or more quarter wavelength ($\lambda/4$) sections as shown in Figure 5. One $\lambda/4$ section is sufficient to match the antenna element to 50 ohms, but several $\lambda/4$ sections can be used to increase the bandwidth of feed transmission line (Reference 7). Carried to an extreme, multiple $\lambda/4$ transmission line sections would approximate a tapered transmission line. The required impedance of a $\lambda/4$ transformer is given by

$$Z_{Transformer} = \sqrt{Z_{in} \times Z_{out}} \qquad (3)$$

Figure 6 shows the use of tapered transmission line and $\lambda/4$ transformer sections for feeding a continuous microstrip radiator.

The second method for feeding the microstrip antenna is shown in Figure 7. In this method the center of the microstrip element is grounded to the ground plane and the coax connector shell is attached to the ground plane while the center conductor of the connector is attached to the microstrip element. The antenna input impedance is a function of the distance from the center and may be selected to be 50 ohms. This method of feeding appears to be more broadband then the edge type feed because the requirement for additional impedance transformation is eliminated.

Radiation Pattern - The radiation pattern of a microstrip antenna is generally like that of an open end waveguide. One of the principle differences is that the H-plane pattern does not have a shape null in the plane of the ground plane. Figure 8 shows a typical E and H-plane pattern for a microstrip antenna. For a given size microstrip antenna, the pattern will show the presence of higher order modes similar to those of a waveguide as the frequency increases and the wavelength decreases.

To a first order, the pattern of a rectangular or square microstrip antenna pattern is composed of radiation from the edge opposite the feed entry and the edge adjacent to the feed. The spacing of these edges are defined by equation (1). As the dielectric constant of the substrate changes, the edge spacing likewise changes and the pattern beamwidth changes. The beamwidth can be calculated by considering the pattern of a two element array given by

$$F(\theta) = 2A \left[\cos \left(\frac{S^\circ}{2} \sin \theta\right)\right] \quad (4)$$

where A is the amplitude of each element (assumed to be equal), $S^\circ$ is the element spacing (obtained from equation (1)),in electrical degrees, and $\theta$ is the angular displacement from a direction normal to the plane of the elements. Typical beamwidths for several dielectric constants are shown in Table I.

TABLE I

TYPICAL MICROSTRIP ANTENNA BEAMWIDTH

| SUBSTRATE $\varepsilon r$ | BEAMWIDTH (DEGREES) |
|---|---|
| 1.0 (AIR) | 60 |
| 1.5 | 76 |
| 2.0 | 90 |
| 2.5 | 106 |
| 3.0 | 120 |

The pattern of a circular microstrip antenna is similar to that square element. It can be calculated by considering an element spacing of A $\sqrt{\pi}$, where A is the radius of the circular element.

The beamwidth is also affected by the ground plane size. Increasing the size of the ground plane above the minimum requirement for estimating back radiation narrows the beamwidth. However, the literature does not give a formula for estimating the ground plane size effect. Therefore, radiation pattern measurements are necessary to determine the beam narrowing effect for each configuration of interest.

Radiation patterns similar to those of annular slot or $\lambda/4$ stub antennas (i.e., a toroidal shaped pattern) can be obtained by feeding a circular element in the center. Figure 9 shows a typical pattern in any plane orthogonal to the plane of the antenna for a center fed configuration. The polarization of this pattern is vertical (i.e., parallel to the plane of the pattern).

Polarization - The microstrip antenna has linear polarization for a single feed as shown in Figure 1. Circular polarization can be obtained by feeding adjacent sides of a square element with a 90° phase difference or a circular element by separating the feeds 90°. Figure 10 shows typical CP feed systems for a circular element using a power divider and a 90° hybrid.

Figure 11 shows a two probe feed system based on the method shown in Figure 6 for obtaining circular polarization. This method requires an additional power divider or hybrid external to the antenna to get the required phase between feeds. Howell measured about 25 dB isolation between the feeds. The radiation pattern for the dual probe configuration (Figure 12) shows excellent results. Howell obtained ARs of only 2 dB at 90° from the beam center.

An alternate method for obtaining CP is shown in Figure 13. The two "ears" which extend away from the circular radiating element, diagonal A, have the effect of creating a conjugate input impedance relative to that of the orthogonal direction, diagonal B. By feeding the radiating element at the midpoint between the diagonals, the impedances are added in parallel and the reactive components cancel yielding a real input impedance (see Reference 6 for examples). The conjugate diagonal impedances yield quadrature excitation currents, and, therefore, a CP radiation pattern.

Impedance - The input impedance for a rectangular or square microstrip radiator according to Munson is approximately 120 ohms at the feed point for an element width of one-half wavelength. The impedance at each radiating edge (i.e., gap or slot) is 240 ohms. The microstrip element can be treated as a low impedance (1 to 10 ohms) microstrip transmission line approximately one-half wavelength long. The half wave transmission line essentially puts the two radiating slots in parallel and results in the 120 ohm input impedance. This value compares closely with Munson's (P.C.) measured results. The details for calculating the exact impedances are given in Reference 1, which is reproduced in Appendix II.

Bandwidth - The bandwidth is the major limitation of the microstrip antenna. The dominating factor is the low transmission line characteristic impedance (1 to 10 ohms) between the two radiating slots. Munson indicates that typical bandwidths for a 0.079 cm (1/32 in.) substrate thickness at 1.0 to 2.5 GHz are about 1% for a 2:1 input VSWR. The bandwidth can be increased by increasing the substrate thickness since the equivalent transmission line impedance increases with the thickness, t, as given by

$$R_o = 120\pi \frac{t}{W\sqrt{\epsilon_r}}, \quad \frac{W}{t} > 10 \tag{5}$$

where W is the width of the microstrip antenna. An emperical formula for the bandwidth (Munson, P.C.) is

$$\text{Bandwidth (MHz)} = 4 f^2 \frac{t}{(1/32)} \quad (\text{VSWR} < 2:1) \tag{6}$$

where f is the frequency in GHz and t is the substrate thickness in inches. The 1/32 factor is convenient to retain since the double clad circuit board is normally fabricated in increments of 1/32 in. (0.079 cm).

Figure 14 shows some measured values of bandwidth as a function of thickness. Additional bandwidth data is given in Appendix I for a number of microstrip antennas having various shapes, substrate thicknesses, and operating frequencies. This data shows bandwidths ranging from 0.9 to 3.5% based on a VSWR of 3:1.

Efficiency - There is very little reported in the literature on the efficiency of the microstrip antenna. Munson (Reference 1) shows the measured gain of an X-band array of microstrip elements (0.079 cm (1/32 in.) substrate) equal to theoretical maximum less the losses of the feed system transmission line. Both Munson (P.C.) and Kaloi (P.C.) report microstrip element efficiencies of 80 to 90%. The sources of loss are the substrate material dissipation factor (loss tangent) and thickness, and the microstrip element losses due to copper conductivity or copper roughness. The substrate thickness probably has the greatest effect on the efficiency. For example, at 400 MHz, the use

of a 0.079 cm (1/32 in.) substrate ($\varepsilon_r$ = 2.5) thickness results in an efficiency of about 65% whereas a 0.318 cm (1/8 in.) substrate thickness would result in an efficiency of about 85%.

Power Handling Capability - No mention is made of power breakdown or power handling capacity in the literature. Power breakdown tests were conducted on the microstrip antenna proposed for SAEP application (Reference 8). No breakdown was detected at 395.35 MHz with a power of 50 watts (average) applied and the pressure reduced from room ambient to 42.6 $N/m^2$ ($4.2 \times 10^{-4}$ atm). The later pressure is slightly below the critical pressure where minimum breakdown power should occur. Munson (P.C.) reports peak pulse powers in the kilowatt range for microstrip antenna elements designed for use at 1 to 10 GHz. Howell (P.C.) reports testing of UHF microstrip with a power of 80 watts (average) applied through the critical pressure region.

The power handling capacity of the microstrip antenna can be increased substantially by coating the surface over the radiating element with a layer of dielectric material to: (1) capture electrons (attachment) in its field and prevent them from generating ions; and (2) provide a smooth surface which keeps the voltage gradients to a minimum. According to Munson (P.C.), paints have been tried but tend to absorb moisture and change dielectric properties. The best results were obtained by laminating a layer(s) of cloth similar to that of the substrate to the antenna surface. This matches the physical properties of substrate and provides a smooth surface, which also tends to improve power breakdown characteristics. Munson (P.C.) reports a breakdown power improvement of 2-1/2 times using a Teflon-fiberglass laminate 0.397 mm (1/64 in.) thick. The dielectric coating also affects the resonant frequency of the microstrip antenna. However, the change is small and can be compensated for in the design process.

Weight - The weight of the microstrip antenna is primarily dependent on the density of the dielectric material used for the substrate. For most designs, double clad circuit board is a satisfactory material for fabrication. The copper is 3.56 or 7.11 $\times 10^{-3}$ cm (1.4 or 2.8 $\times 10^{-3}$ in.) thick on each side. Except for very thin substrates, the copper is a small part of the total weight. The weight of a 0.079 cm (1/32 in.) circuit board (Teflon-fiberglass substrate) is

1.83 kg/$m^2$ (.0026 lbm/$in.^2$). Weights for other circuit board thicknesses can be calculated by using this figure as a base. The weight of a UHF microstrip antenna fabricated from 0.318 cm (1/8 in.) circuit is about 0.9 kg (2 lbs.). A minimum weight condition for the SAEP application may be obtained by considering the SAEP aft heat shield for the dielectric substrate and adding conducting surfaces appropriately.

# ENVIRONMENTAL EFFECTS

This section discusses the effects of some of the expected SAEP environments as related to the performance of a microstrip antenna.

## General

The principle effects of the SAEP mission environments are related to the effects of a particular environment on the electrical properties of the dielectric substrate or on the atmosphere surrounding the electric fields of the antenna. These effects can be controlled to some extent by choosing materials which are stable in the environment, selecting design features which allow for the shortcomings of the selected materials, and excluding an undesirable atmosphere by appropriate techniques

## Temperature

The principle effect of heating the microstrip antenna to an elevated temperature is a change in dielectric constant of the substrate. Figure 15 shows data from 3M for their K-6098 copper clad stripline laminate which was used for the proposed SAEP microstrip antenna. The loss tangent also changes but has no significant effect on the microstrip antenna because of the maximum magnitude is relatively low. For a temperature change from 294 to 344°K (70 to 160°F), the data in Figure 15 shows the dielectric constant decreases from 2.423 to 2.416. From equation (1) we can obtain

$$f_2 = f_1 \frac{\sqrt{\varepsilon_{r_1}}}{\sqrt{\varepsilon_{r_2}}}$$

$$= 395.50 \frac{\sqrt{2.423}}{\sqrt{2.416}}$$

$$= 396.07 \text{ MHz.}$$

This gives a frequency change ($f_2 - f_1$) of 0.57 MHz.

Using the data of Kaloi in Figure 2, a frequency change of 0.66 MHz was predicted by considering the slope of a cross plot of frequency versus dielectric constant assuming a 0.318 cm (1/8 in.) substrate thickness.

## High Energy Radiation

The effects of high energy radiation are limited to comparing before and after effects (Reference 9) since the nature in which the radiation levels are supplied do not usually permit measurements during radiation. Information about recent radiation tests performed by NASA-GSFC were obtained from Robert Munson (Ball Brothers Research Corporation) for three different substrate materials. The test articles had the following microstrip antenna parameters:

(a) Design Frequency - 4 GHz

(b) Size

1.588 cm (5/8 in.) square radiating patch
3.810 cm (1-1/2 in.) square circuit board and ground plane
0.079 cm (1/32 in.) circuit board thickness

The radiation type and dosage is given in Table II. One test article of each substrate material received all the particle radiation dosage and one of each substrate material received the gamma radiation dosage.

The resonant frequency shift measured by Ball Brothers after the radiation exposure is given in Table III. The frequency shifts can be related to changes in dielectric constant which can then be used to estimate the frequency change for the SAEP application at 400 MHz. The frequency shift at 400 MHz can be obtained by dividing the values in Table III by 10. The worst case is a 0.6% frequency change. The frequency shift caused by this radiation is opposite that caused by a temperature increase.

The Gamma radiation caused some delamination of the microstrip antenna backside and at one corner of the radiating patch of the antenna fabricated from K-6098. However, the antenna still functioned at the reduced frequency. Since the delamination was observed at just one point, it is possible that

TABLE II

HIGH ENERGY RADIATION TEST ENVIRONMENT

| PARTICLE TYPE | ENERGY (mev) | FLUENCE (part/sq cm) | DOSE (rads) | FLUX (parts/sq cm/sec) |
|---|---|---|---|---|
| Protons | 0.3 | $4 \times 10^{14}$ | $2.7 \times 10^{9}$ | $2 \times 10^{10}$ |
| Protons | 1.0 | $7.5 \times 10^{11}$ | $2.4 \times 10^{6}$ | $2 \times 10^{10}$ |
| Protons | 2.0 | $4 \times 10^{10}$ | $7.9 \times 10^{4}$ | * |
| Electrons | 0.3 | $3 \times 10^{15}$ | $1.1 \times 10^{8}$ | $2 \times 10^{11}$ |
| Electrons | 1.0 | $3 \times 10^{14}$ | $9.0 \times 10^{6}$ | $2 \times 10^{10}$ |

GAMMA - in air - cobalt 60 source

LEVEL - Dose Rate = $520 \times 10^{3}$ rads/hr

FLUX = $2.8 \times 10^{12}$ $\gamma/cm^2$ s

EXPOSURE - Duroid and K-6098 200 hr

Polyguide 100 hr

* Determined by time required for turning accelerator on and off (on time estimated at about 5 sec).

TABLE III

RADIATION TEST DATA - FREQUENCY SHIFT (MHz)

| | Radiation Type | |
|---|---|---|
| Material | Gamma | Particulate |
| Duroid | -27 | -4 |
| K-6098 | -23 | 0 |
| Polyguide | -15 | -9 |

Note: Frequency shift relative to 4 GHz.

it was not due entirely to the radiation.

The radiation exposure experienced by an antenna will be highly dependent on the particular mission and geometrical and material (shielding) configurations. The environment given in Table IV was used as an example of exposure for comparison with the measured data. This environment corresponds to a Jupiter probe mission using the Pioneer 10 results for the Jupiter radiation environment where shielding against low energy particles including the solar wind is provided by the aft heat shield.

TABLE IV
SAMPLE OUTER PLANET MISSION ENVIRONMENT

| ENVIRONMENT | FLUENCE (particles/$cm^2$) | DOSE (rads) | ($gm/cm^2$) |
|---|---|---|---|
| Solar Flare Protons | $5 \times 10^9$ (E > 30 MeV) | $1.2 \times 10^3$ | 1.1 |
| Jupiter Protons | $5 \times 10^{12}$ (E > 35 MeV) | $1.1 \times 10^6$ | 1.4 |
| Jupiter Electrons | $4 \times 10^{12}$ (E > 3 MeV) | $1.2 \times 10^5$ | 1.5 |

The radiation exposure to the antenna under this environment will be roughly a uniform dose of $1.2 \times 10^6$ rads at any point within the material. The test samples were 0.079 cm (1/32 in.) thick which corresponds to 0.18 $g/cm^2$.

The application test data from Table III are the 1 MeV electron exposure of $3 \times 10^{14}$ $e/cm^2$ corresponding to $9 \times 10^6$ rads and the $Co^{60}$ gamma exposure of $10^8$ rads for the Duroid and K-6098 samples and $5 \times 10^7$ rads for the Polyguide samples. (NOTE: 1 rad = $3.3 \times 10^7$ 1 MeV electrons/$cm^2$ = $1.9 \times 10^{10}$ $Co^{60}$ gamma rays/$cm^2$.) These radiations are penetrating enough to produce the approximately uniform dose profile. The additional particulate exposures add progressively higher doses to the surface of the samples. For example, the low energy protons provide a surface dose of $2 \times 10^9$ rads for a depth of less than 0.25 μm.

The 1 MeV electron exposure is roughly eight times the $1.2 \times 10^6$ rads Jupiter probe environment while the gamma ray exposures exceed the probe dose by factors of four to eight. Thus the measured electrical changes should be an upper limit to those expected for this sample case.

## Pressure

The primary effect of low pressure (space vacuum) is outgassing of the dielectric substrate. This could change the dielectric constant of the substrate, but the degree is likely to be extremely small compared to the effects of either temperature or radiation. A review of the consistituent of Teflon filled fiberglass does not reveal any evidence of outgassing sufficient to

cause a change in electrical properties. Both Teflon and glass are inert at the modest temperature of the SAEP mission.

The pressure environment during the operation of the microstrip antenna in the SAEP mission is $3.04 \times 10^3$ N/m$^2$ (0.03 atm) and greater. These pressures are above that for minimum voltage breakdown. At $3.04 \times 10^3$ N/m$^2$ (0.03 atm), the breakdown power should be several times greater than the 50 watts obtained at critical pressure (Reference 8).

## Saturn/Uranus Atmosphere

An antenna breakdown test is warranted for a candidate outer planet probe antenna because: (1) the link for the communications will probably require fairly high powers thus infering a possibility of breakdown; and (2) there appears to be little analytical work on breakdown in typical outer planet atmospheres - Hydrogen Helium with traces of water, methane, Neon and Ammonia.

A review of the literature (References 10 through 14) did not show a simple technique for making a quantative estimate of the effects of the outer planet atmospheres on the proposed SAEP microstrip antenna breakdown characteristics. Voltage breakdown of gaseous conductors is determined by the charge production rate and the charge depletion rate. The charge production rate herein is primarily governed by electron collisions. Ion collisions are less efficient due to the lower ion mobilities. Radiation charge production is insignificant as the domain of interest is at the lower atmosphere - as opposed to the ionosphere where radiation is the dominant production mechanism. Similarly thermal ionization, as in entry plasmas, is not a significant generation mechanism for this problem. Concentrating on electron collisions, a charge production rate for an outer planet atmosphere could be formulated.

The charge depletion rate is governed by diffusion, attachment and recombination. Diffusion (the ionization "wandering away" from the domain of interest) may not be a dominate mechanization herein as the bulk of the transmission will occur at the denser portion (postentry) of the atmosphere.

Attachment (electrons attaching to neutrals (or the "walls") then being neutralized by ions) will probably be the major depletion mechanism because of the dense atmosphere - transmission after blackout - and because of the confines of the aft heat shield. Direct recombination is usually not a dominant mechanism, however it does vary markedly with trace contaminants.

A theoretical formulation of the production and depletion rates for candidate outer planet atmospheres will benchmark the validity of tests; e.g., assuring no trace contamination. The tests in turn will feedback data to extend the theory where fundamental information is lacking or obscure. The tests should generally show lower breakdown levels than seen in air as roughly indicated by Figure 16 (Figure 5.8 of Brown) and Table V (Table 4.3 of Cobine).

TABLE V

MEAN ENERGY REQUIRED TO PRODUCE AN ION PAIR BY AN ELECTRON IMPACT*

| | EFFECTIVE IONIZATION POTENTIAL, VOLTS | |
|---|---|---|
| Gas | U** = 0.5 $(10)^3$ - 1 $(10)^3$ e.v. | U Greater Than 4 x $10^3$ e.v. |
| Air | 45 | 32.4 |
| $H_2$ | 36 | |
| He | 31 | |
| Ne | . | 43 |

* See Table 4.3, Reference 10
** U = Electron Energy

## Aging

A review of the aging properties of the microstrip antenna substrate (Teflon-fiberglass) does not reveal any changes due to aging in a space vacuum environment. The properties of alternate substrate materials should be checked for similar properties before designing an antenna for long term space flight.

## Insulation Cover

The effect of a thermal insulation cover over the microstrip antenna is a function of the dielectric constant and loss tangent of the insulation. The insulation proposed of the SAEP has both a low dielectric constant (1.04) and loss tangent (.0002). The results of the temperature tests reported in the next section show the effect of a cover with similar characteristics on radiation pattern and impedance is insignificant. The literature does not contain data which can readily be used for an analytical prediction of cover effects.

An insulation cover, bonded to the radiating surface of a microstrip antenna, could significantly increase the minimum breakdown power, since the insulation material is also a dielectric material. Although the pressure inside the insulation, a urethane foam, will equalize to ambient pressure, the leakage rate is high and would not result in partial pressures within the foam cells conducive to breakdown. However, even with adverse partial pressures inside the foam cells, the improved attachment conditions created by the presence of the foam cell walls would be expected to significantly increase the minimum breakdown power of the microstrip antenna.

## TEMPERATURE TESTS

This section discusses the results of radiation pattern and VSWR measurements made with a microstrip antenna temperature at room ambient and at 344°K (160°F). These measurements were made to determine the effect of temperature on the resonant frequency, the axial ratio, AR, and the AR bandwidth (AR $\leq$ 2 dB at pattern peak). The antenna proposed for SAEP was used for these tests.

### General

Radiation pattern and VSWR measurements were made with the microstrip antenna temperature at room ambient and at 344°K (160°F). The latter is the maximum temperature the antenna is expected to see during the SAEP mission. The microstrip antenna (Figure 4) and ground plane were covered with a low density foam (ETHAFOAM - 35.2 kg/m$^3$ (2.2 lbm/ft$^3$)) 1 in. thick with electrical properties equivalent to insulation material (ECCOFOAM SH - 32.0 kg/m$^3$ (2.0 lbm/ft$^3$)) considered for the SAEP. Table VI gives the electrical properties of these two materials. The properties of these two materials are so close that the test results using either should be essentially identical. The simulated insulation was used in these tests because the literature did not contain information suitable for analytical evaluation of the effect.

TABLE VI
ELECTRICAL CHARACTERISTICS

| Material | $\varepsilon_r$ | tan $\delta$ |
|---|---|---|
| ETHAFOAM (220) | 1.05 | .001 |
| ECCOFOAM SH | 1.04 | .0002 |

## Test Setup

The microstrip antenna was mounted in the center of a 82.55 cm (32.5 in.) diameter ground plane. The 82.55 cm (32.5 in.) ground plane is equivalent to the SAEP diameter and was used for previous measurements (Reference 8). Three thermocouples equally spaced around the antenna were attached to the radiating surface of the antenna and three on the back side of the ground plane directly opposite the surface thermocouples. One additional thermocouple was placed on the back side of the ground plane directly behind the center of the antenna. Figure 17 shows the relationship of the thermocouple to the edge of the antenna. The thermocouple junctions were attached to 3.18 cm (1/8 in.) square nichrome ribbon pads to ensure sufficient contact area. The temperatures were measured sequentially by a Minimite instrument. The simulated insulation was held in place by double backed tape around the antenna. The tape was not used over the antenna because of a lack of adhesion to Teflon tape covering the surface of the microstrip antenna.

Heat was applied to the back side of the ground plane by three heat lamps. The lamp voltages were each controlled by a Variac. The desired temperature was approached slowly in order to reach equilibrium condition when the peak temperature of 344 (+6, -0)°K (160 (+10, -0)°F) was measured by the surface thermocouples on the antenna. The equilibrium temperature conditions were very stable and permitted adequate time to make the desired electrical measurements. The temperature variation of the thermocouples was only about 5°F.

The electrical measurements were made in a large anechoic chamber. The test setup for the VSWR measurements is shown in Figure 18. The frequency was varied by a swept frequency generator, VSWR measured by a reflectometer and recorded by a rectangular plotter. Figure 19 shows the test article mounted on a tower for radiation pattern measurements. The patterns were measured using rotating linear polarization in order to obtain the shape and axial ratio simultaneously.

VSWR Measurements - VSWR measurements were measured first to establish the resonant frequency for the radiation pattern measurements. The VSWR of the microstrip antenna at room temperature and without the simulated insulation cover is shown in Figure 20. The addition of the simulated insulation increased the resonant frequency about 0.05 MHz as shown by Figure 21. With the temperature of the antenna at 344°K (160°F), Figure 22 shows the resonant frequency increased to 396.8 MHz, an increase of 1.3 MHz. The two dips in the VSWR plots are attributed to the maximum and minimum dimension of the antenna.

Radiation Pattern Measurements - The radiation patterns of the microstrip antenna at room ambient temperature are shown in Figure 23. The patterns measured at 395.11 and 395.92 MHz represent the edges of the AR bandwidth (AR < 2 dB at pattern peak). The patterns at the same frequencies (Figure 24) with the temperature of the antenna raised to 344°K (160°F) shows an increase in AR at 395.11 and 395.50 MHz but only a small increase in AR at 395.92 MHz. The circular gain, however, only decreased 0.5 dB at 395.50 MHz (the resonant frequency at room temperature) and remained essentially unchanged at 395.92 MHz. It is also interesting to note that the AR at angles away from the beam center decreased, the reverse of the AR characteristics at room temperature.

Patterns measured at the 344°K (160°F) resonant frequency (396.65 MHz) and AR bandwidth edges (396.25 and 297.05 MHz) are shown in Figure 25. These patterns are essentially identical to the corresponding patterns measured at room temperature.

Patterns measured to determine the effects of the simulated insulation (2.54 cm (1 in.) thick) are shown in Figure 26. There is no significant difference in pattern shape or AR.

The symmetry of the patterns about the normal to the antenna, at 45° from the normal, is shown in Figure 27. This pattern was measured during the testing reported in Reference 8.

Discussion of Results - The frequency shift indicated by the VSWR measurements was 1.3 MHz. The frequency shift indicated by the pattern measurements was 1.15 MHz. This is a difference of 0.15 MHz, most of which can be accounted for by the tolerance of the temperature control.

The radiation patterns show that the simulated insulation has no significant effect on the characteristics of the microstrip antenna. Bonding the insulation to the antenna could have an advantageous effect of increasing the power handling capacity of the antenna by: (1) providing a dielectric coating over the antenna; and (2) keeping the external Saturn/Uranus environment (i.e., constituent gases) away from the high electric field strengths of the microstrip antenna, thereby negating these potential effects.

The results of the radiation pattern measurements at 344°K (160°F) show a shift of 1.15 MHz. The frequency shift based on the change in substrate dielectric constant, based on 3M's published data, is 0.57 MHz as shown in the section on ENVIRONMENTAL EFFECTS, under Temperature. This is about half of the frequency shift measured. The difference is attributed to the difference in the actual material as compared to smooth published data. The 3M material (and likely the Roger's material can be purchased with measurements at room and elevated temperatures on material taken from the material ordered. However, the pattern and VSWR characteristic at the upper edge of the AR band do not show a significant change in circular gain. Therefore, it appears that the microstrip antenna could be tuned so that the desired operating frequency extend slightly above the upper AR band edge. Then, as the temperature increases, the resonant frequency of the antenna passes through and beyond the operating frequency but stays within the AR bandwidths.

Alternatively, a more broadband version of the CP microstrip antenna can be designed using a hybrid or power divider as discussed in the section on DESIGN CONSIDERATIONS. This would have no impact on the SAEP design as presently configured since the added circuitry could be added without change in size or weight of the microstrip antenna currently proposed for the SAEP.

# CONCLUSIONS

The microstrip antenna is an ideal antenna for the SAEP application. It is compact and can meet the high "g" environment for entry in the outer planet atmospheres. The electrical performance of the microstrip antenna is well behaved and to some degree can be configured to control gain and pattern beamwidth. Wideband circularly polarized microstrip antenna designs are available which have improved performance in the SAEP environment compared to that of the antenna proposed.

## ACKNOWLEDGEMENTS

The author expresses his appreciation to J. Q. Howell of NASA's Langley Research Center, R. E. Munson of Ball Brothers Research Corporation, and C. M. Kaloi of the Naval Missile Center and for information and numerous discussions about the microstrip antenna. Appreciation is also expressed to C. A. Hinrichs of MDAC-E for discussion and preparation of the subsection on the Saturn/Uranus Atmosphere, and R. L. Kloster of MDAC-E for discussions and assistance in preparation of the subsection on Radiation.

## REFERENCES


1 Munson, R. E.: Conformal Microstrip Antennas and Microstrip Arrays. IEEE Transactions and Propagation, AP-22, No. 1, January 1974.

2 Howell, J. Q.: Microstrip Atennas. 1972, G-AP International Symposium Digest, December 1972.

3 Howell, John Q.: Microstrip Antennas. Accepted for publication in IEEE Transactions on Antennas and Propagation

4 Munson, R. and Murphy, L.: Conformal Microstrip Array for a Parabolic Dish. Abstracts of the Twenty-Third Annual Symposium, USAF Antenna Research and Development Program, October 1973.

5 Munson, R.: Microstrip Phased Array Antennas. Abstracts of the Twenty-Second Annual Symposium, USAF Antenna Research and Development Program, October 1972.

6 Kraus, J. D.: Antennas, McGraw Hill, 1950, p. 427, Figure 14-35F.

7 Anon: Reference Data for Radio Engineers, Fifth ed., Howard W. Sams and Company (New York) 1969, p. 583.

8 Anon: Saturn/Uranus Atmospheric Entry Probe, Part III Electrical and Electronic Systems (NAS 2-7328), McDonnell Douglas Astronautics Company - East, Final Report MDC E0870, 18 July 1973.

9 Harrison, W. E. Jr.: Effects of Radiation on Electronic Component and Materials. EDN, November 1963.

10 Cobine, J. D.: Gaseous Conductors, Dover Publications, Inc. (New York) 1958.

11 Brown, S. C.: Basic Data Of Plasma Physics, John Wiley & Sons, Inc. (New York) 1959.

12 MacDonald, A. D.: Microwave Breakdown in Gases, John Wiley & Sonc, Inc. (New York) 1966.

13 Taylor, W. C., Scharfman, W. E. and Moritz, T: Voltage Breakdown of Microwave Antennas. Advances in Microwaves, Academic Press, Vol. 7, (New York) 1971.

14 Martin, I.A. and Chown, J.: Study of the Breakdown Characteristics of Antennas in the Atmospheres at Mars and Venus. (NAS 7-100), Stanford Research Institute, Final Report, February 1963.

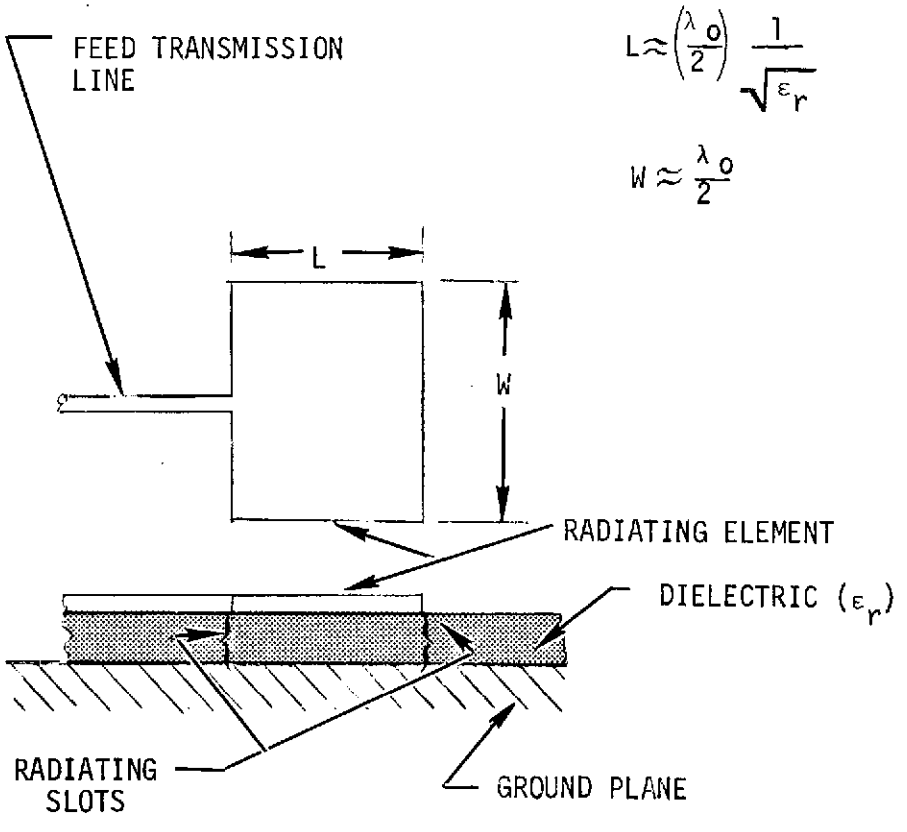


FIGURE 1

BASIC MICROSTRIP ANTENNA

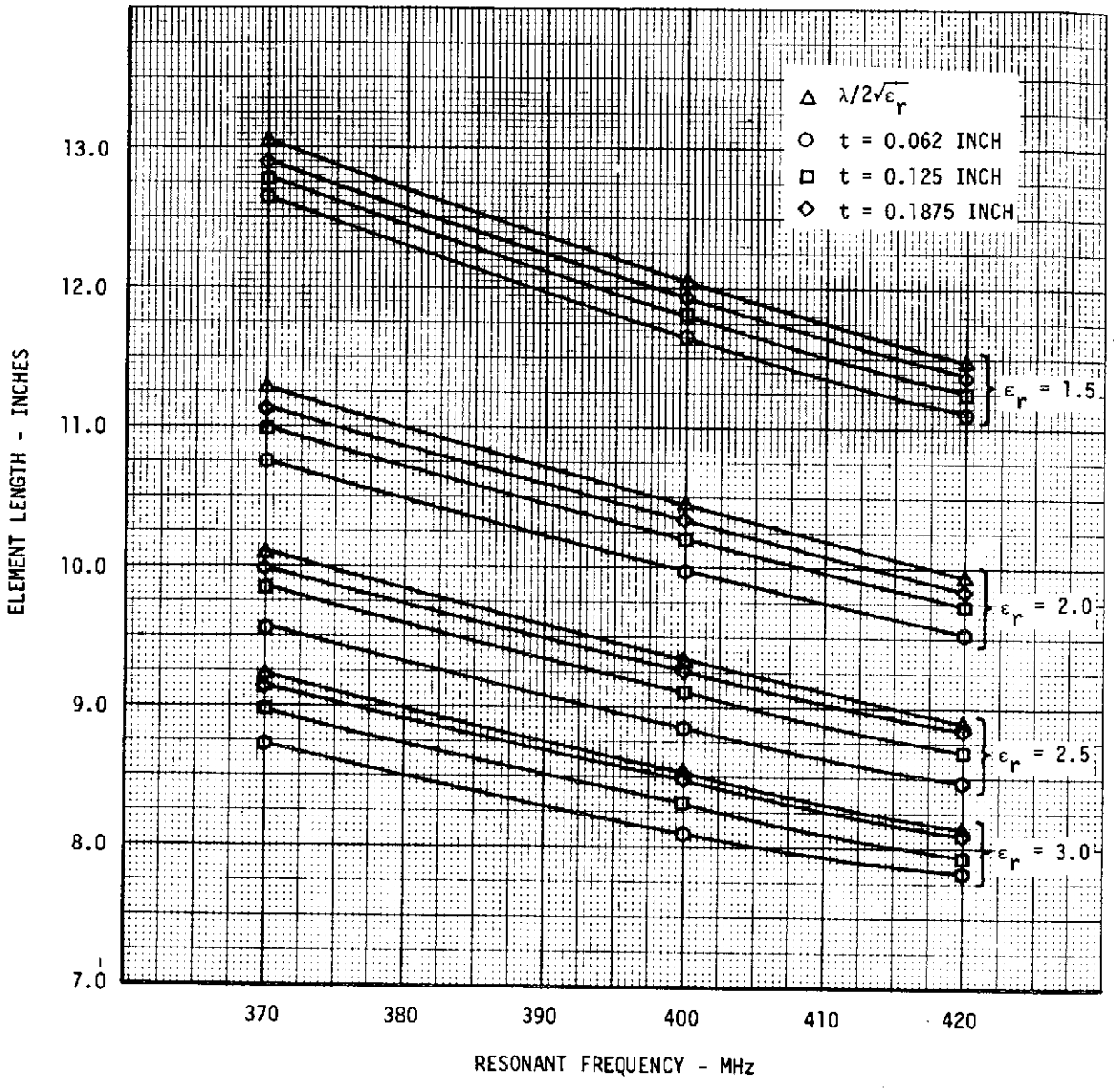


FIGURE 2

MICROSTRIP ANTENNA SIZE CHARACTERISTICS
(DATA COURTESY C. M. KALOI, NMC)

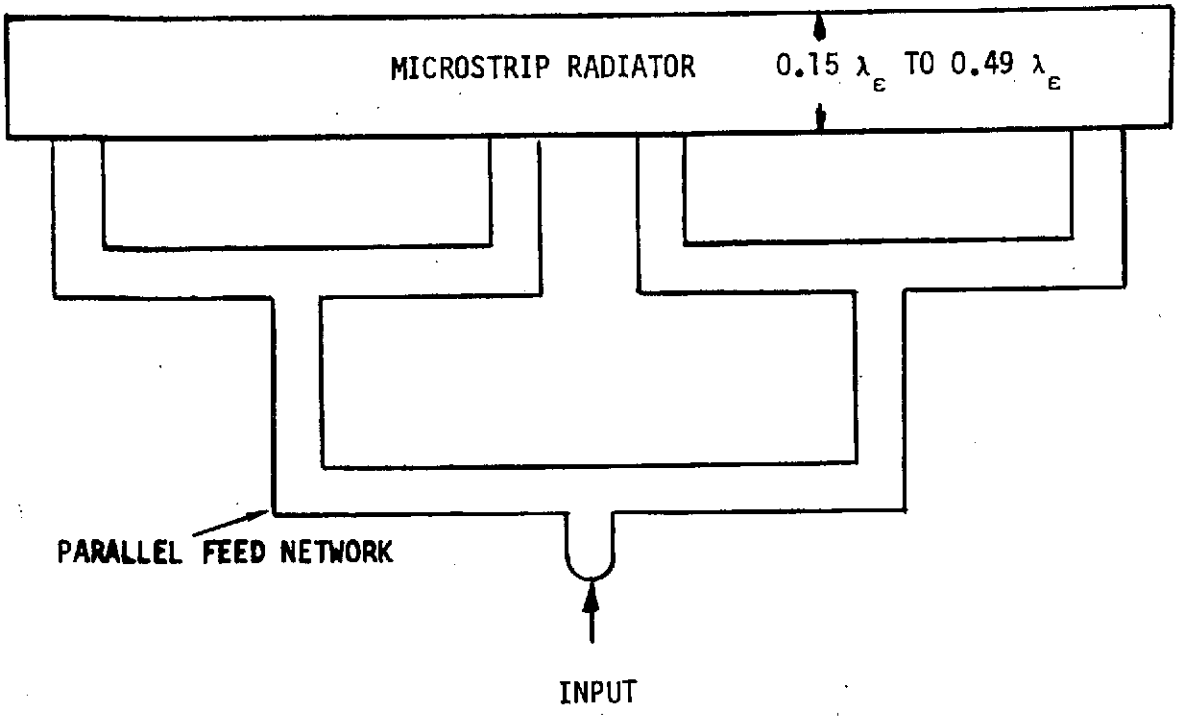


FIGURE 3
MICROSTRIP ANTENNA ARRAY

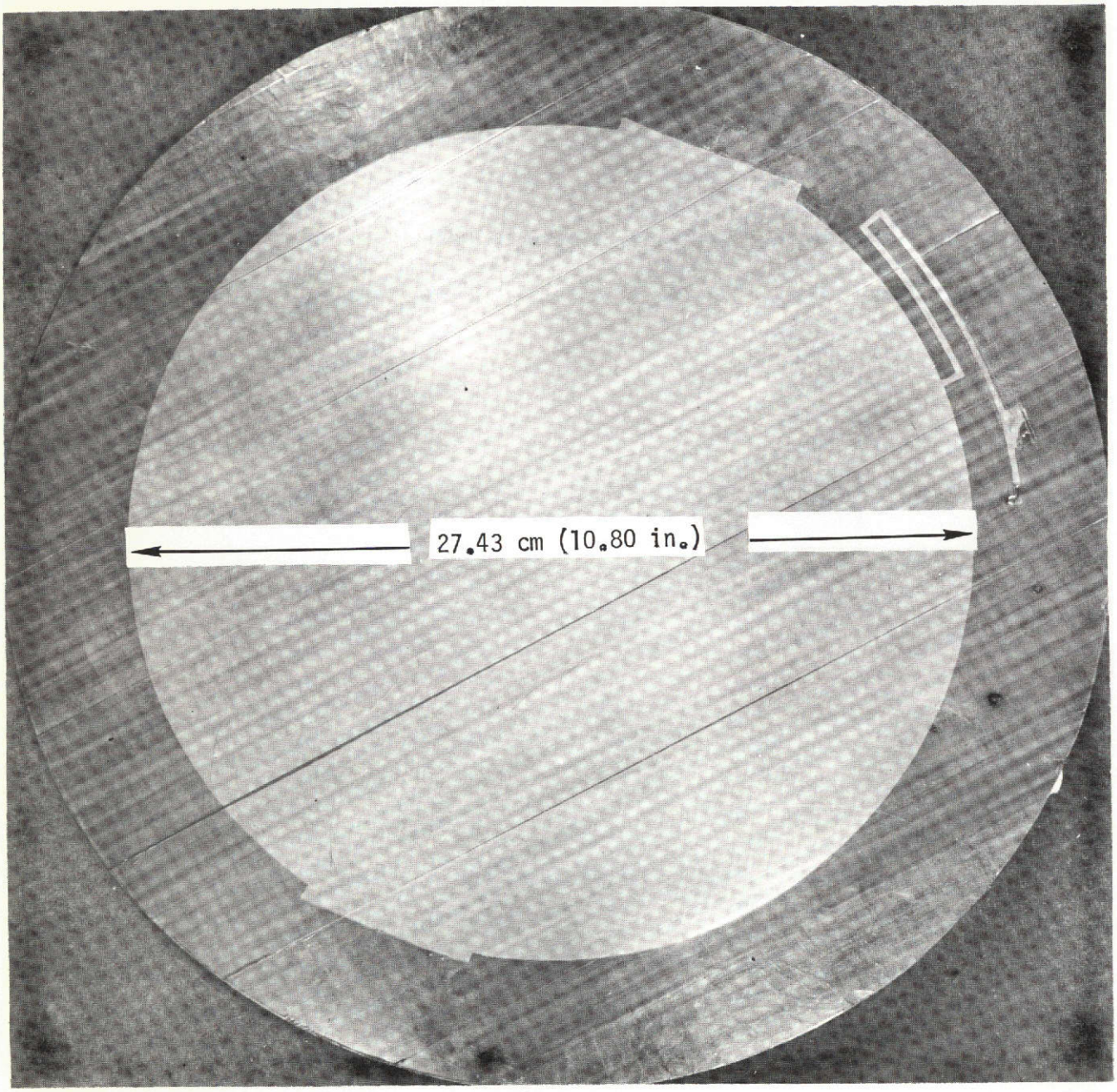


FIGURE 4
MICROSTRIP ANTENNA FOR CIRCULAR POLARIZATION

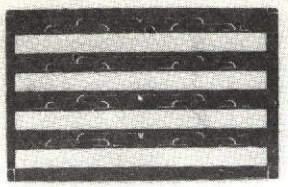

Fig. 7. High gain flat microstrip antenna.

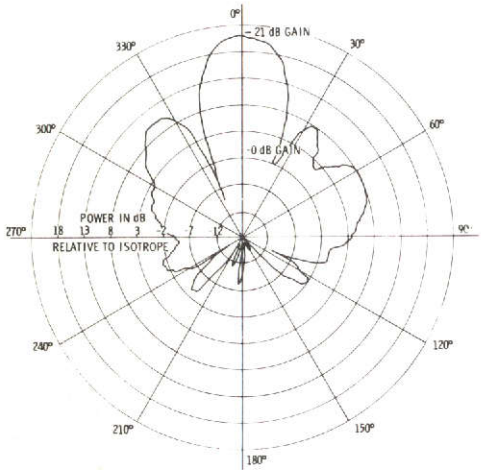


Fig. 8. Gain and pattern of 7.62 cm x 12.7 cm x 0.79 cm microstrip array at 9.92 GHz.

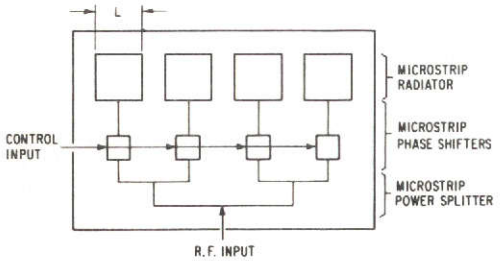


Fig. 9. Electrically scanned microstrip phased array (low cost and low profile).

An experimental model 7.62 cm × 12.7 cm × 0.79 mm (Fig. 7) was built and tested and confirms a gain (Fig. 8) in agreement with the theoretical predictions (Fig. 6). The measured gain of 21 dB is also plotted on the predicted gain curve (Fig. 6). The microstrip antenna offers high gain for a low cost. It also offers a low profile antenna that can operate flush mounted to a metal surface.

## VII. Microstrip Phased Arrays

By adding "pin diodes" for digital phase shifting, Fig. 9, to the microstrip substrate an integrated electrically scanned antenna is attained. The process of phasing the radiators to scan the beam requires breaking up the microstrip radiators into individual elements. The individual microstrip elements (a sample is shown in Fig. 10) work just like the long microstrip radiator described in the previous section. By using $L$ the length of the individual microstrip radiators we can calculate the resonant length, input impedance, and bandwidth of the microstrip radiator just as was done in the previous section.

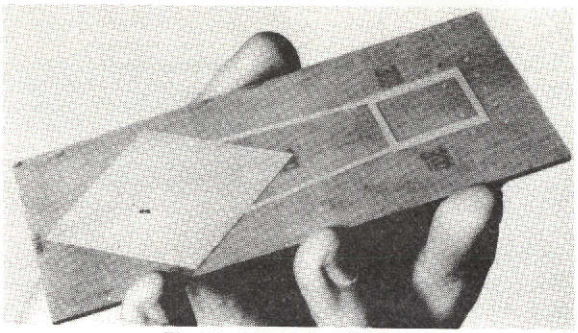

Fig. 10. Microstrip radiator.

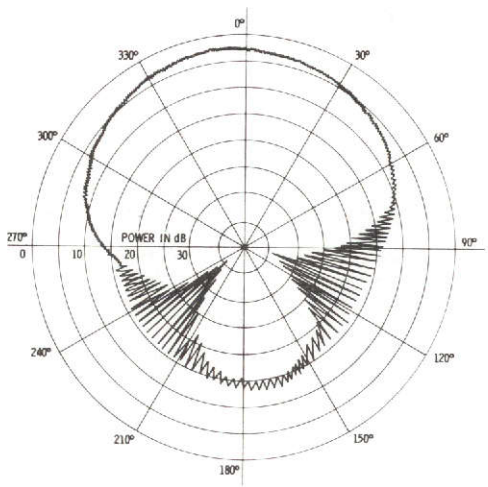


Fig. 11. Radiation pattern of microstrip patch. Patterns were measured with spinning dipole to demonstrate low axial ratios to wide angle.

This works quite well except when the $L$ of the individual radiator is not reduced below 0.25 $\lambda_0$. For $L < 0.25\ \lambda_0$ the radiation resistance of the microstrip radiator rapidly disappears, i.e., the slots $A$ and $B$ are not long enough to match free-space efficiently because their size has been reduced below cutoff for the modes that must be matched to free space as described by Harrington [4, p. 278].

Each of these microstrip radiators are rectangular microstrip elements and each one produces a hemispherical coverage pattern, Fig. 11. A conceptual model of the phased array shown in Fig. 9 was built and tested to demonstrate a complete microstrip electrically scanned phased array. The patterns scanned to the angles predicted with a gain within 1 dB of the expected gain, Fig. 12. The phase shifters used were microstrip 90° hybrid phase shifters with diodes in the two output legs. Driving two diodes in the two output legs of the hybrid changes the phase of the reflected power in the reflected port of the hybrid. The phase shift attained is twice the distance the short reference is moved in the two output legs. Three phase shifters were used in series for each element to produce 0°, 45°, 90°, 135°, 180°, 225°, 270°, or 315° phasing of each element. The phase shifters along with all of their dc feed lines, dc blocks, RF blocks, the RF corporate feed network, the matching network, and the microstrip radiators were all photo etched on one side of one microstrip board.

## VIII. Conclusions

Microstrip antennas constitute a new class of onmidirectional antenna for missiles and satellites. These antennas are capable of producing a predictable and nearly perfect onmidirectional coverage. A new low cost low profile flat microstrip array is shown to have 90-percent aperture efficiency. In addition, the flat microstrip

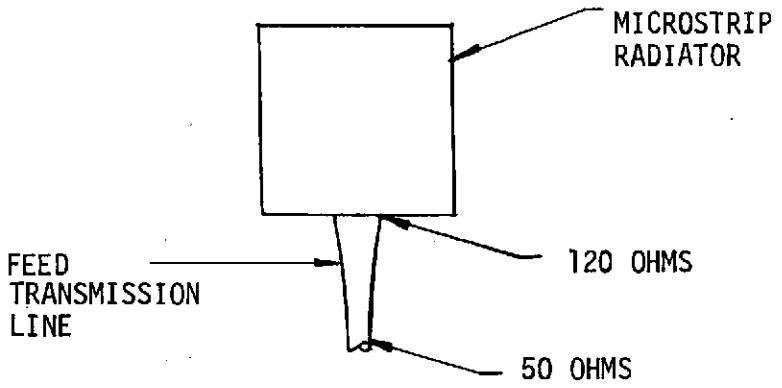


(a) TAPERED FEED TRANSMISSION LINE

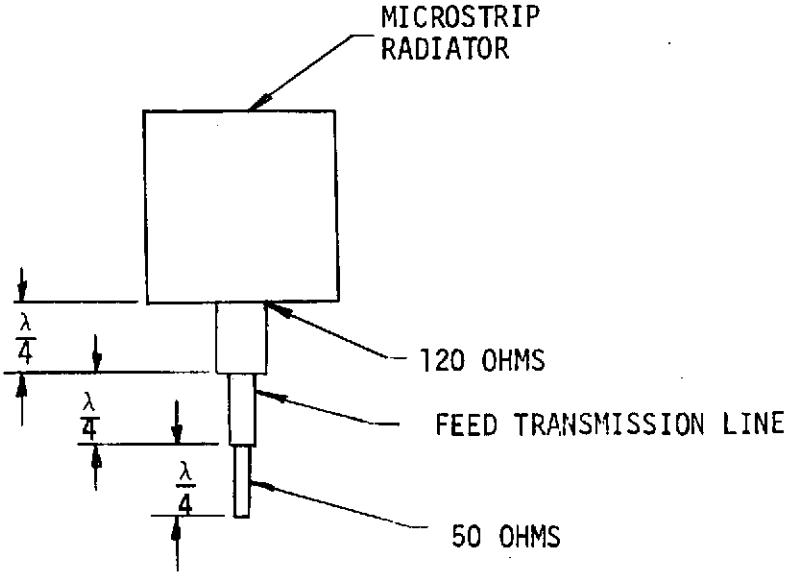


(b) FEED TRANSMISSION LINE WITH MULTIPLE QUARTER WAVE TRANSFORMER SECTIONS

FIGURE 5
FEED SYSTEMS

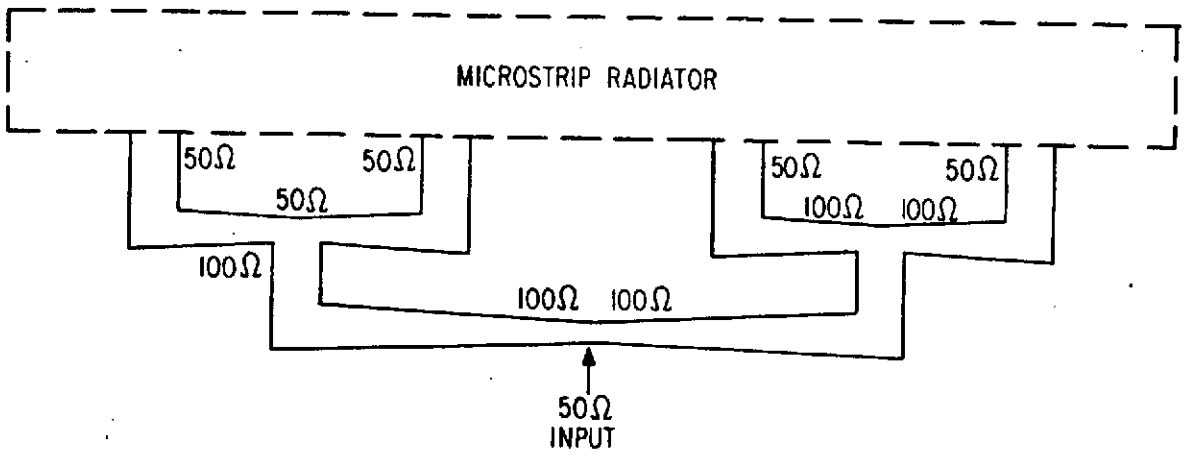


TAPERED LINE METHOD

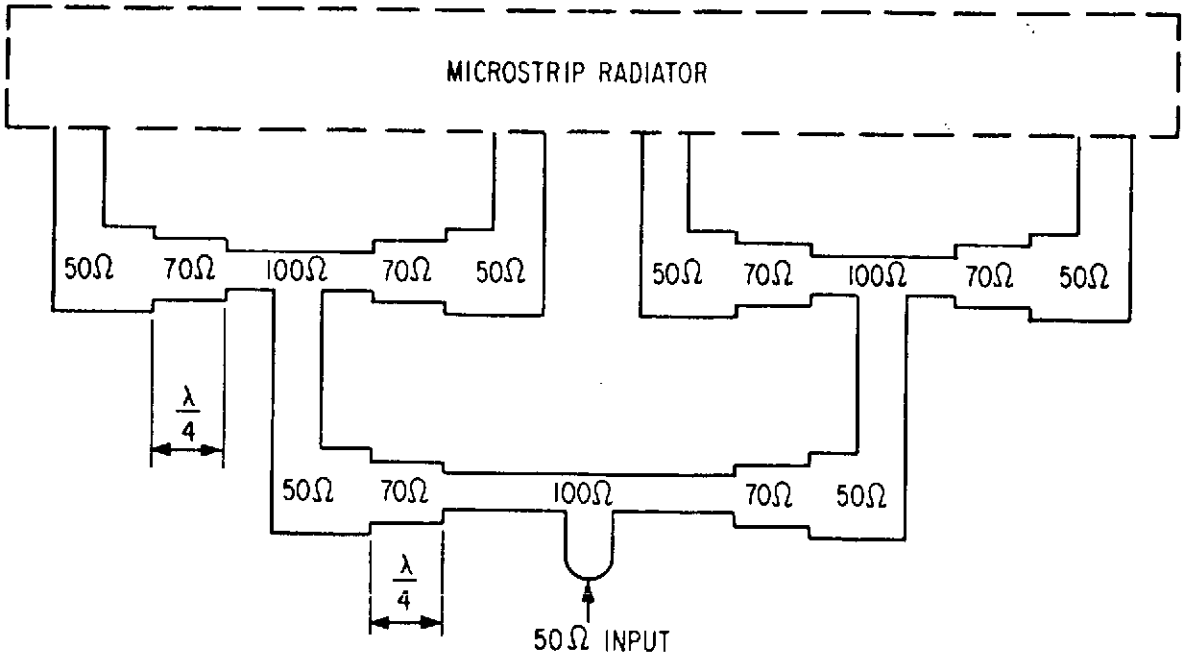


QUARTER WAVE TRANSFORMER METHOD

FIGURE 6

PARALLEL FEED NETWORKS
(COURTESY R. E. MUNSON, BALL BROTHERS RESEARCH CORP.)

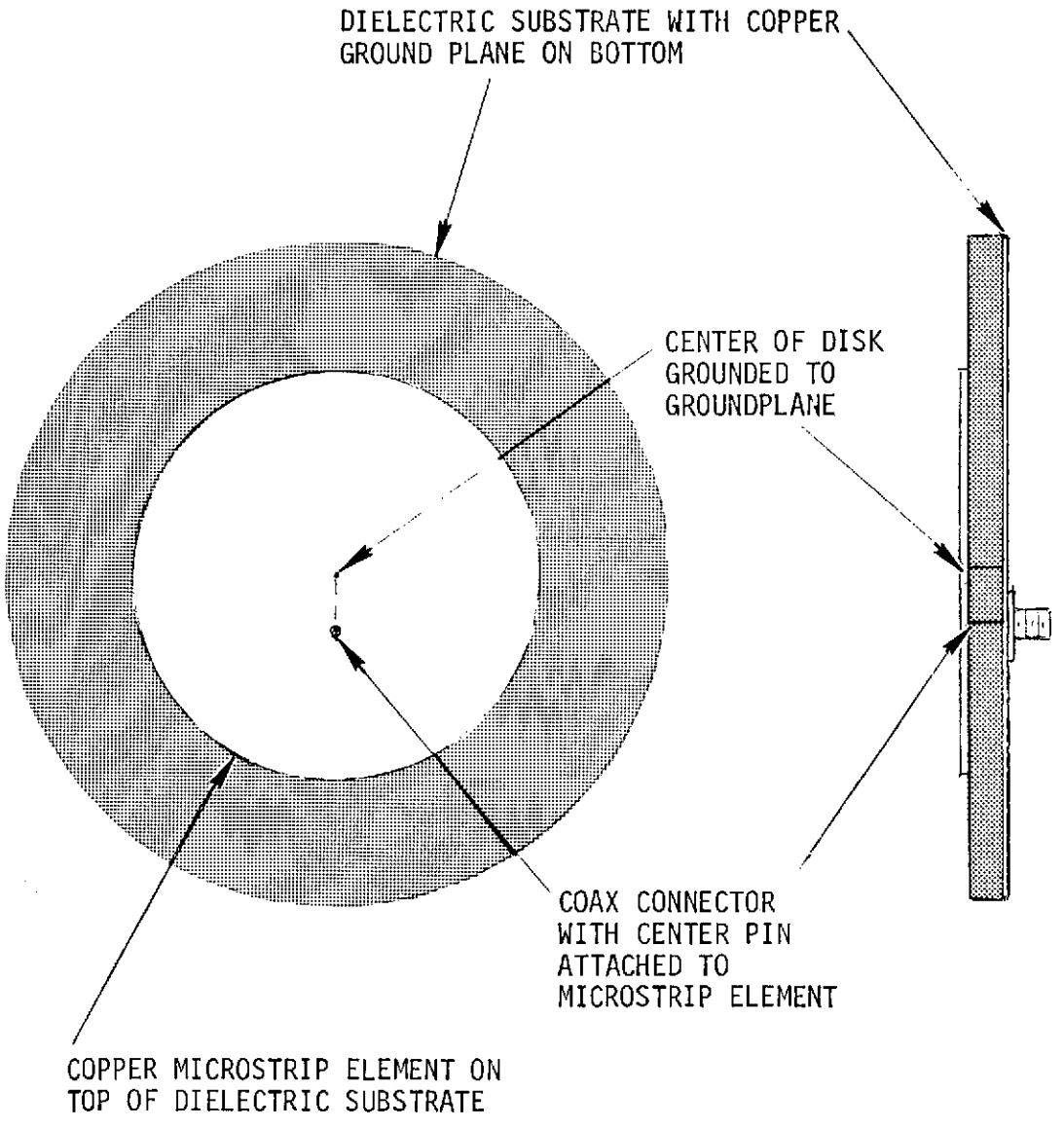


FIGURE 7

CIRCULAR MICROSTRIP ANTENNA WITH CENTER GROUNDED AND FED FROM THE BACK

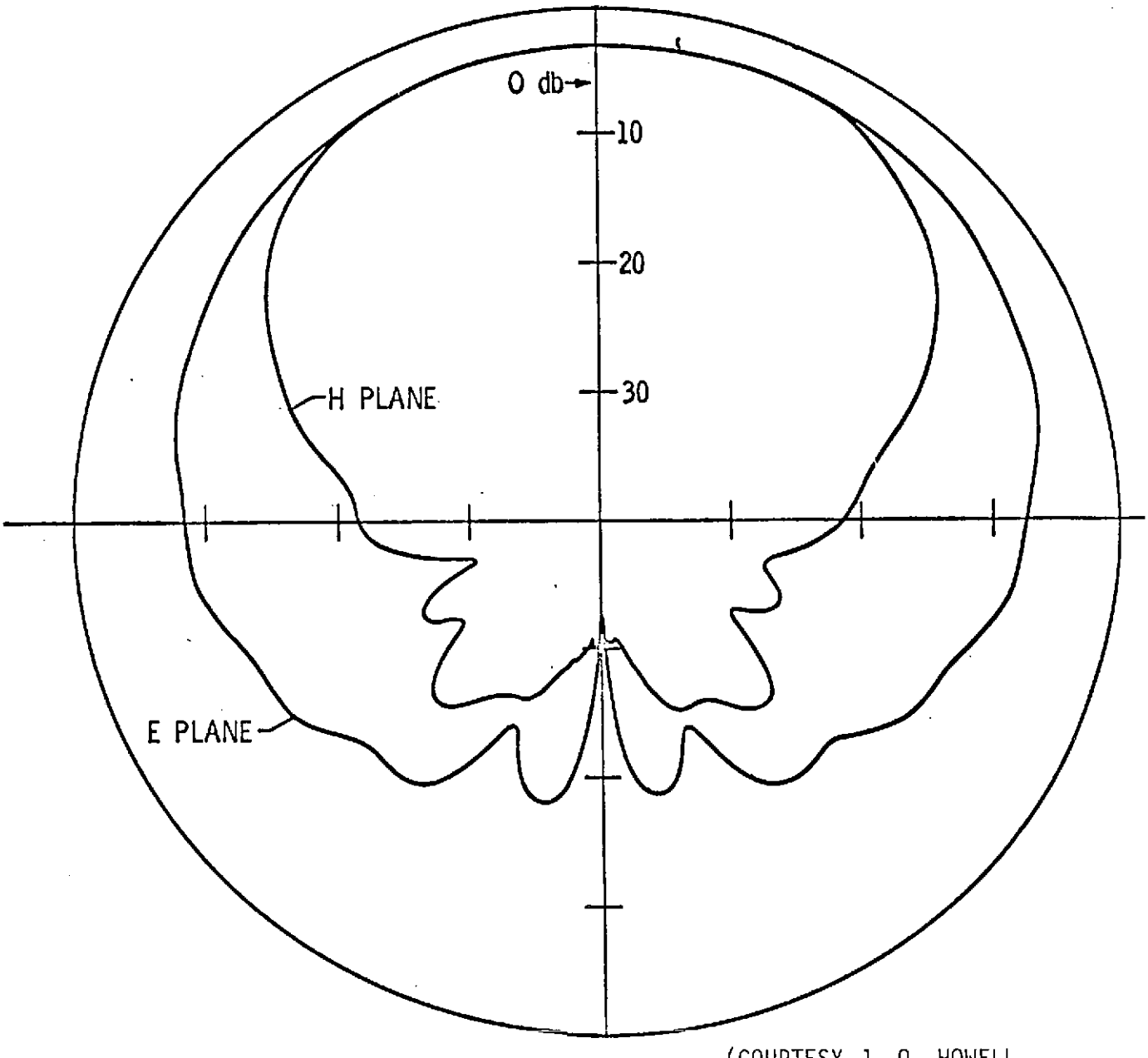


(COURTESY J. Q. HOWELL,
NASA-LaRC)

FIGURE 8

TYPICAL E - AND H - PLANE
PATTERNS OF A MICROSTRIP ANTENNA
(SQUARE ELEMENT, $\varepsilon_r$ = 8.5, FREQ.= 1.7 GHz)

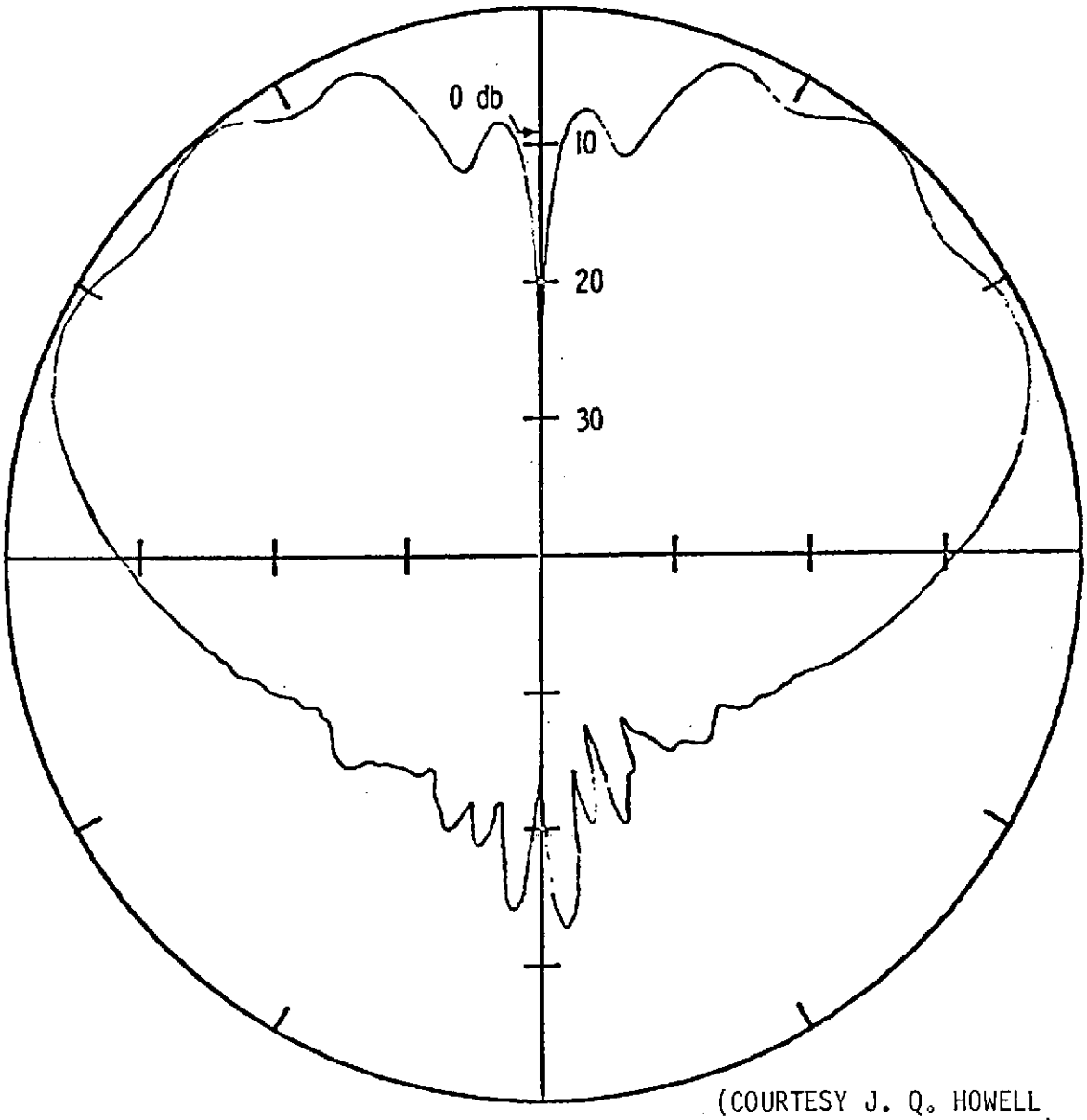


(COURTESY J. Q. HOWELL
NASA-LaRC)

FIGURE 9

TYPICAL PATTERN OF A CENTER FED CIRCULAR MICROSTRIP ANTENNA

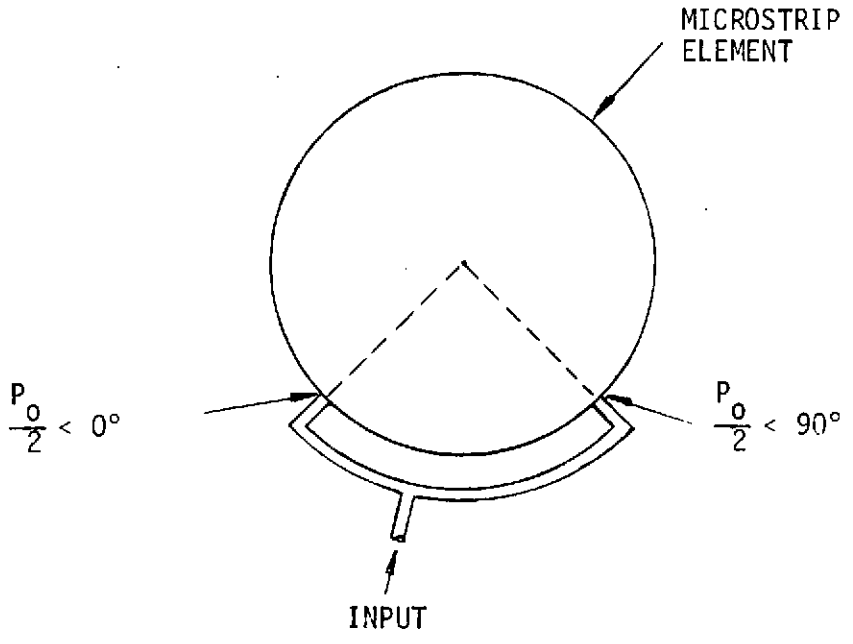


(a) POWER DIVIDER FEED

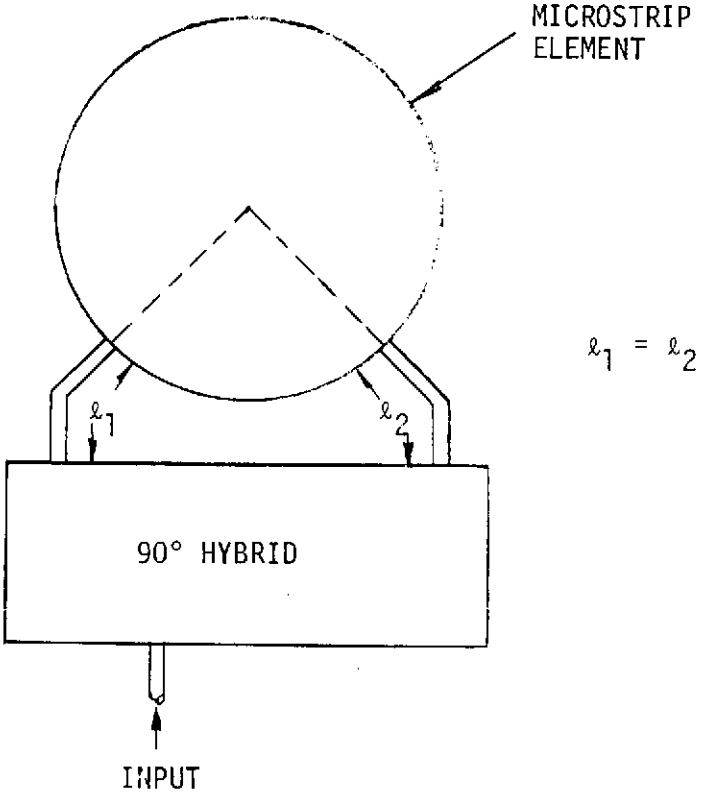


(b) HYBRID FEED

FIGURE 10

FEED METHODS FOR CIRCULAR POLARIZATION

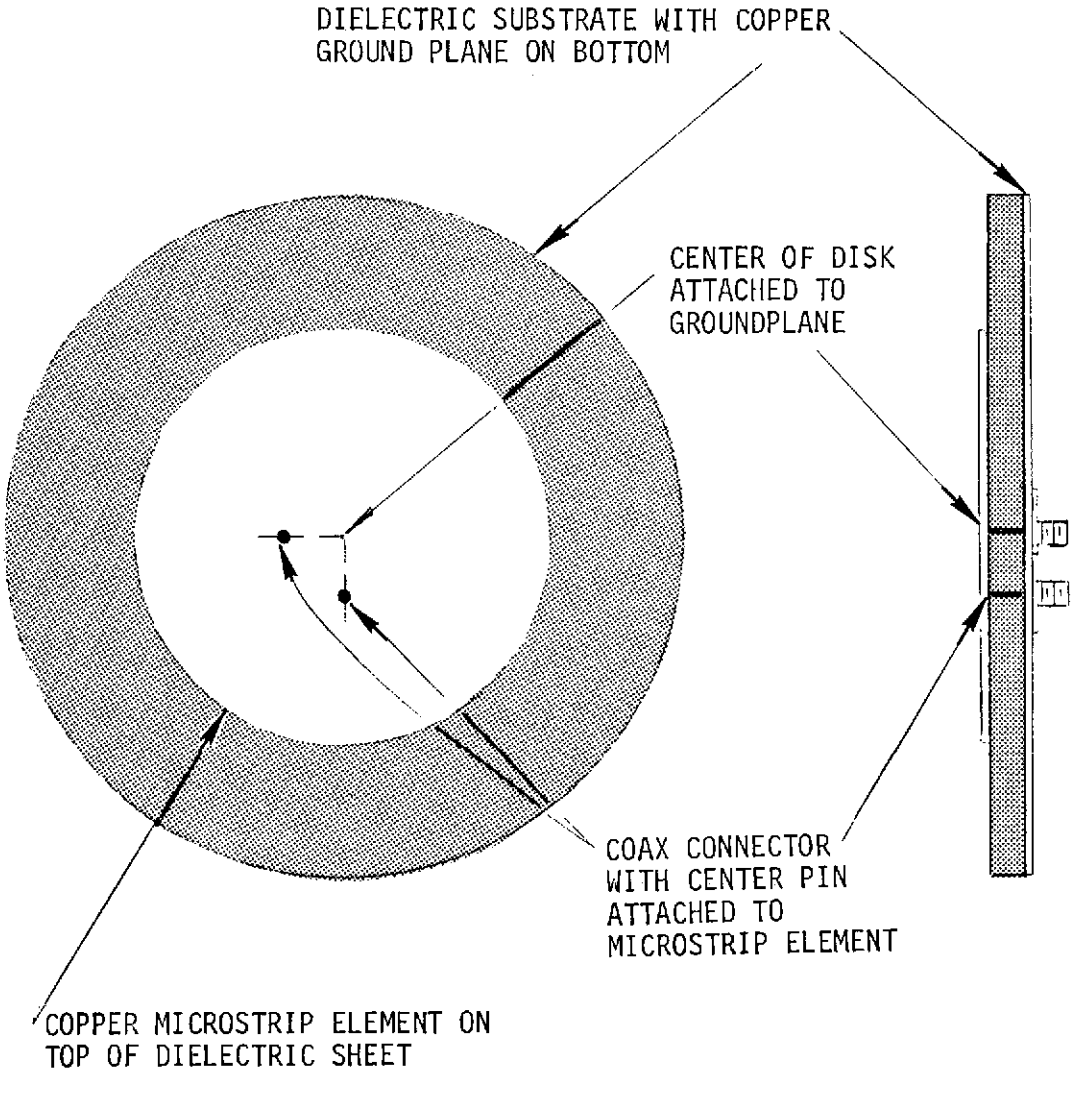


FIGURE 11

CIRCULAR MICROSTRIP ANTENNA WITH FEED CONFIGURATION FOR CIRCULAR POLARIZATION

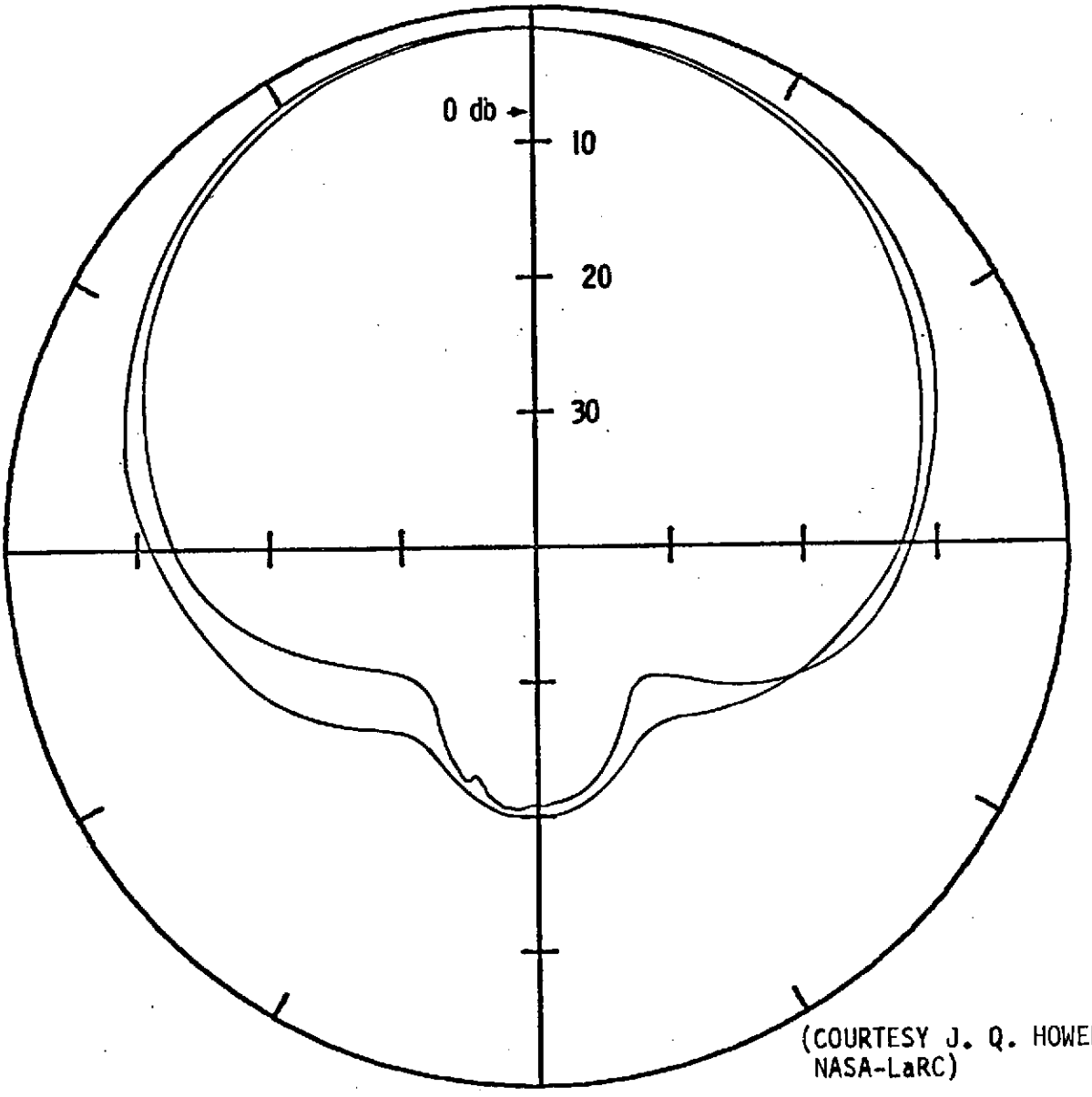


FIGURE 12

UHF ANTENNA RESPONSE TO BOTH HORIZONTALLY
AND VERTICALLY POLARIZED INPUT

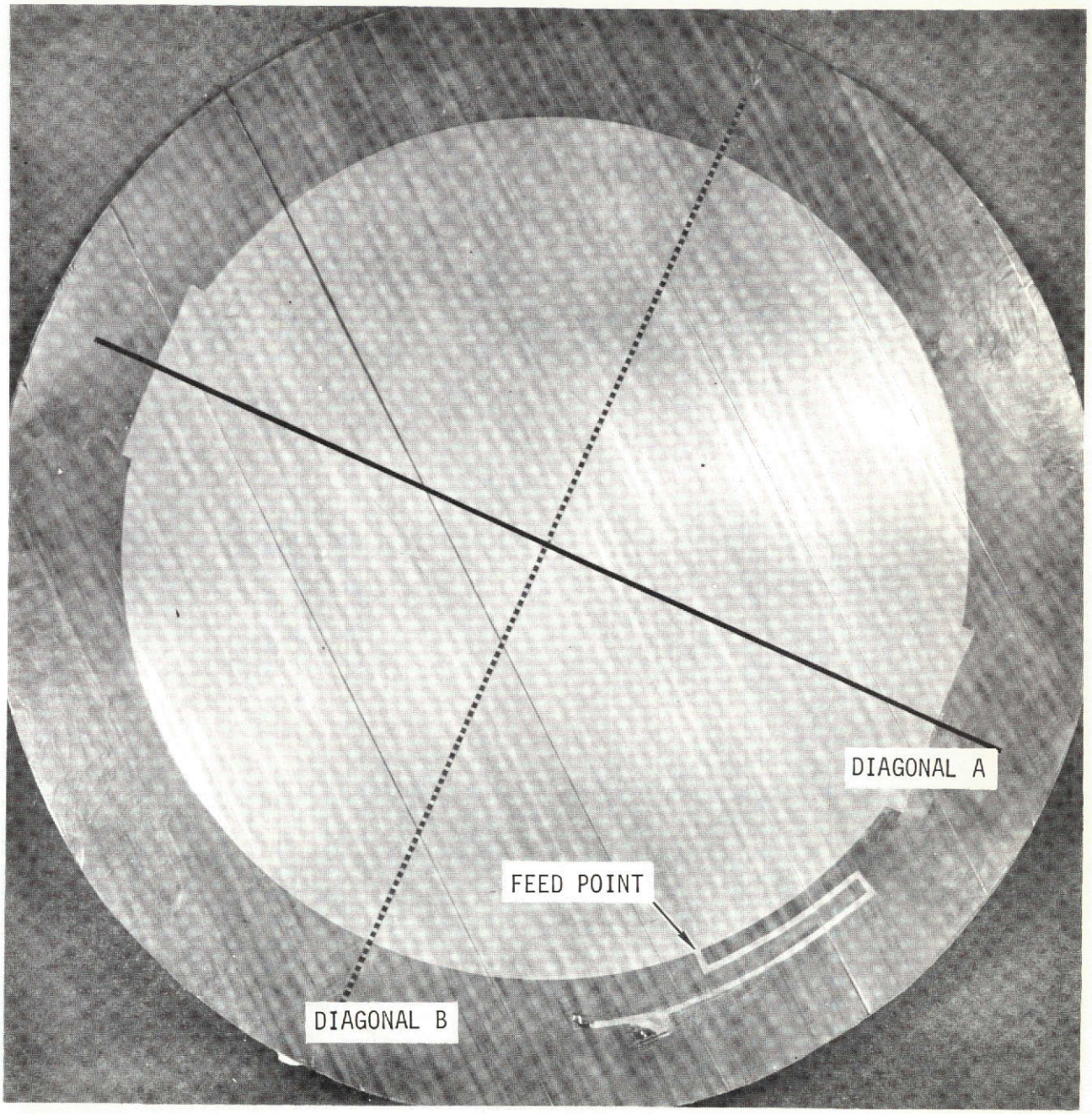


FIGURE 13

PHOTO OF MICROSTRIP ANTENNA-CIRCULAR POLARIZATION WITH SINGLE FEED

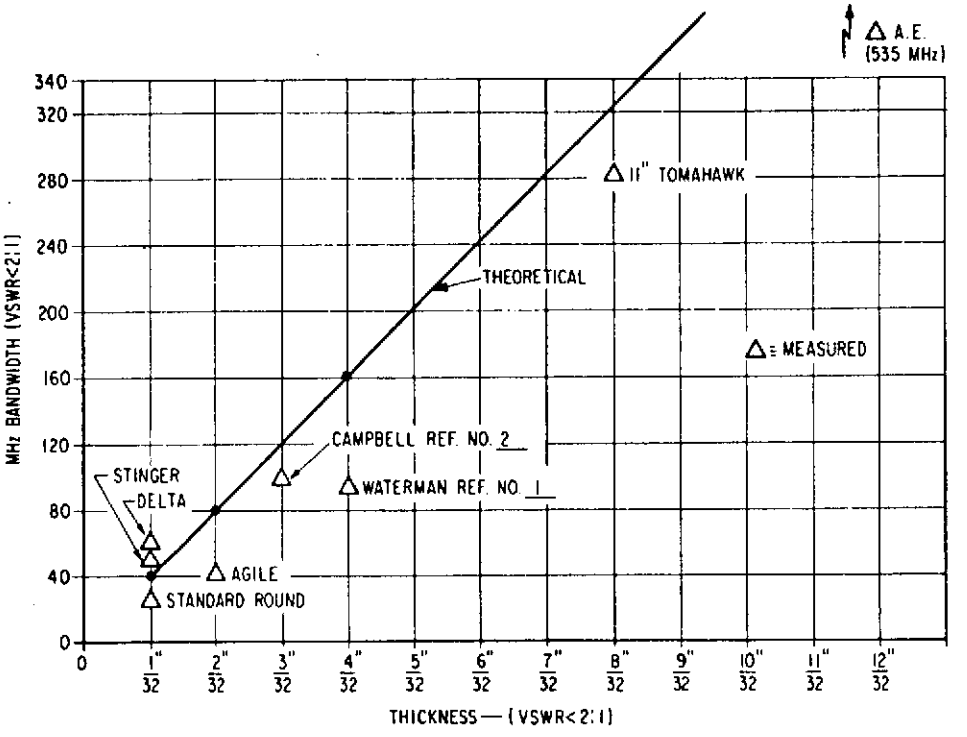


FIGURE 14

MICROSTRIP ANTENNA BANDWIDTH (VSWR<2:1) AS A FUNCTION OF ANTENNA THICKNESS (S-BAND) (COURTESY R. E. MUNSON BALL BROTHERS RESEARCH CORP.)

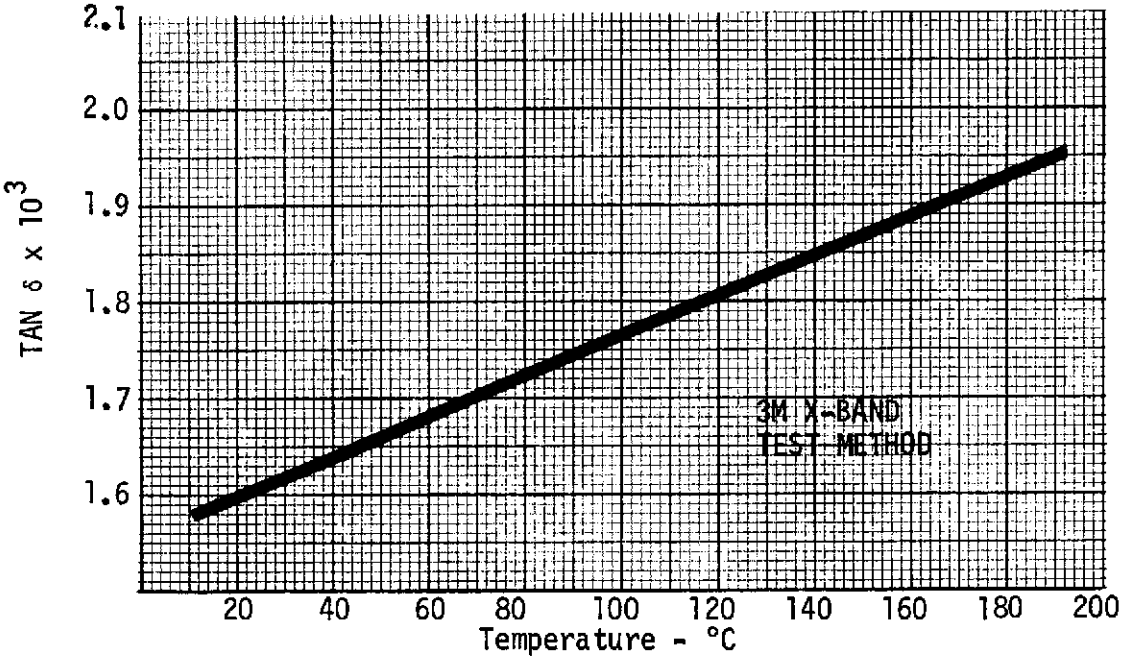


EFFECT OF TEMPERATURE ON DISSIPATION FACTOR - K-6098

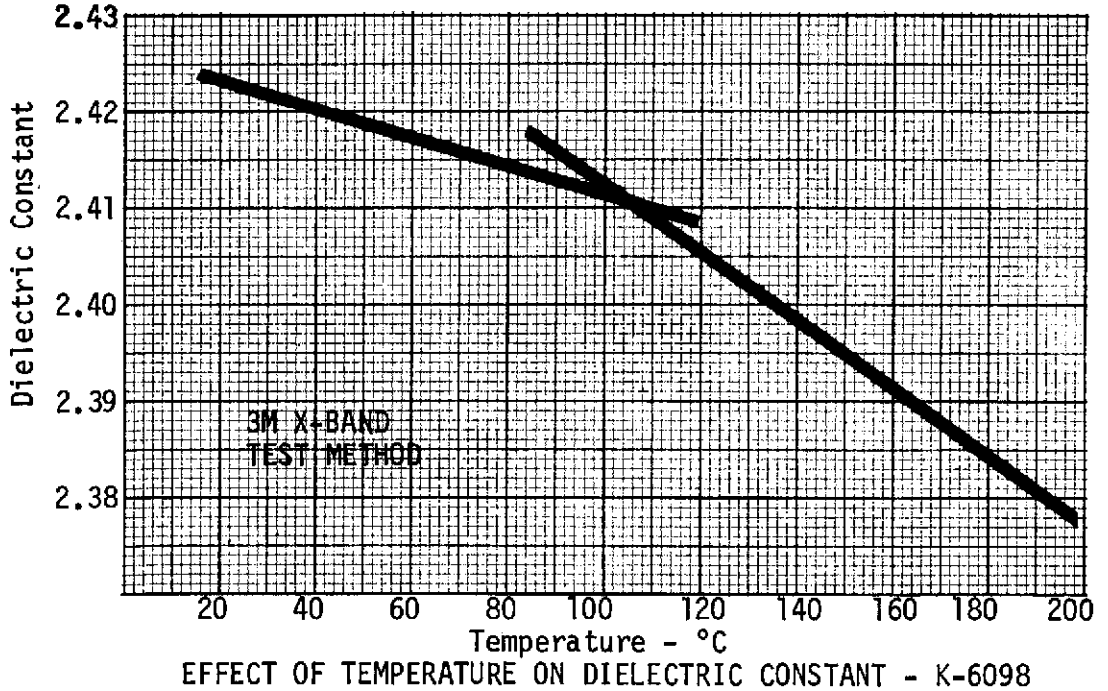


EFFECT OF TEMPERATURE ON DIELECTRIC CONSTANT - K-6098

FIGURE 15
EFFECTS OF TEMPERATURE ON 3M K-6098 (3M DATA)

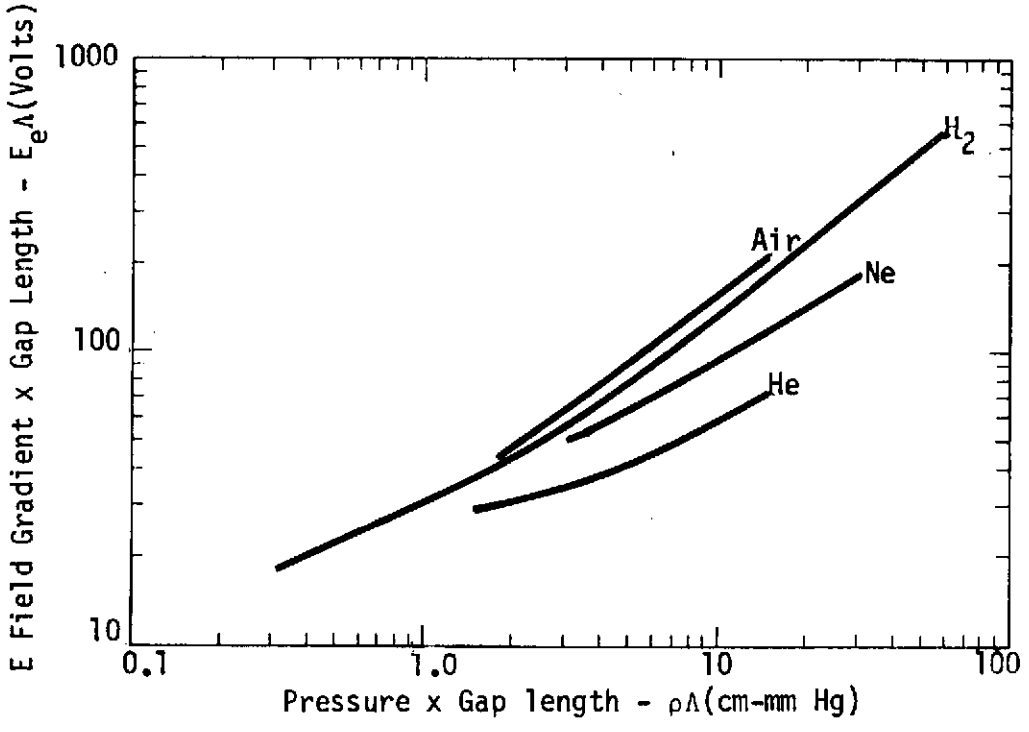


FIGURE 16

PASCHEN CURVES FOR HIGH-FREQUENCY BREAKDOWN IN AIR, $H_2$, Ne and He.

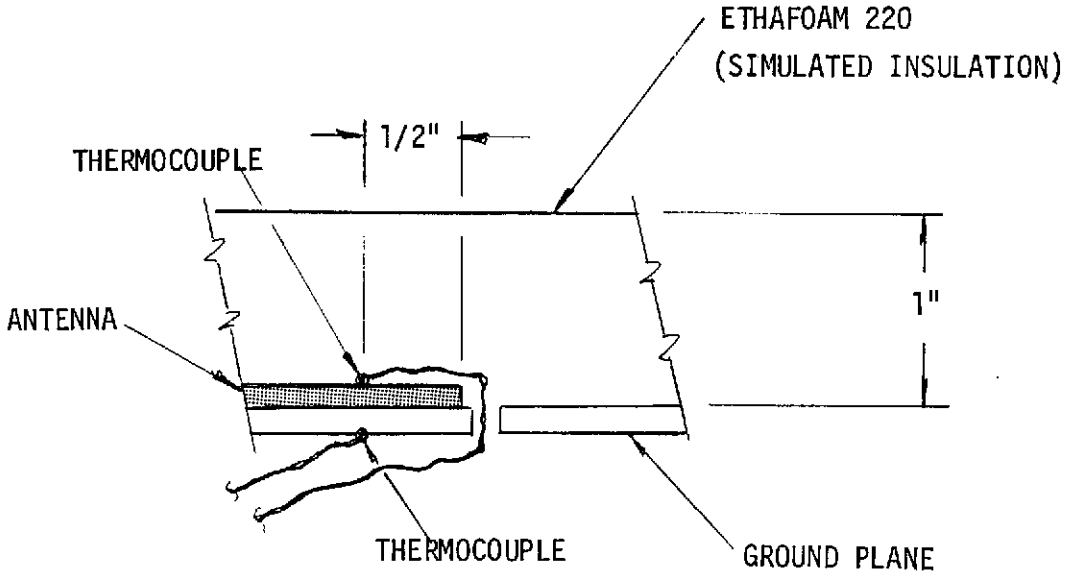


FIGURE 17
THERMOCOUPLE CONFIGURATION

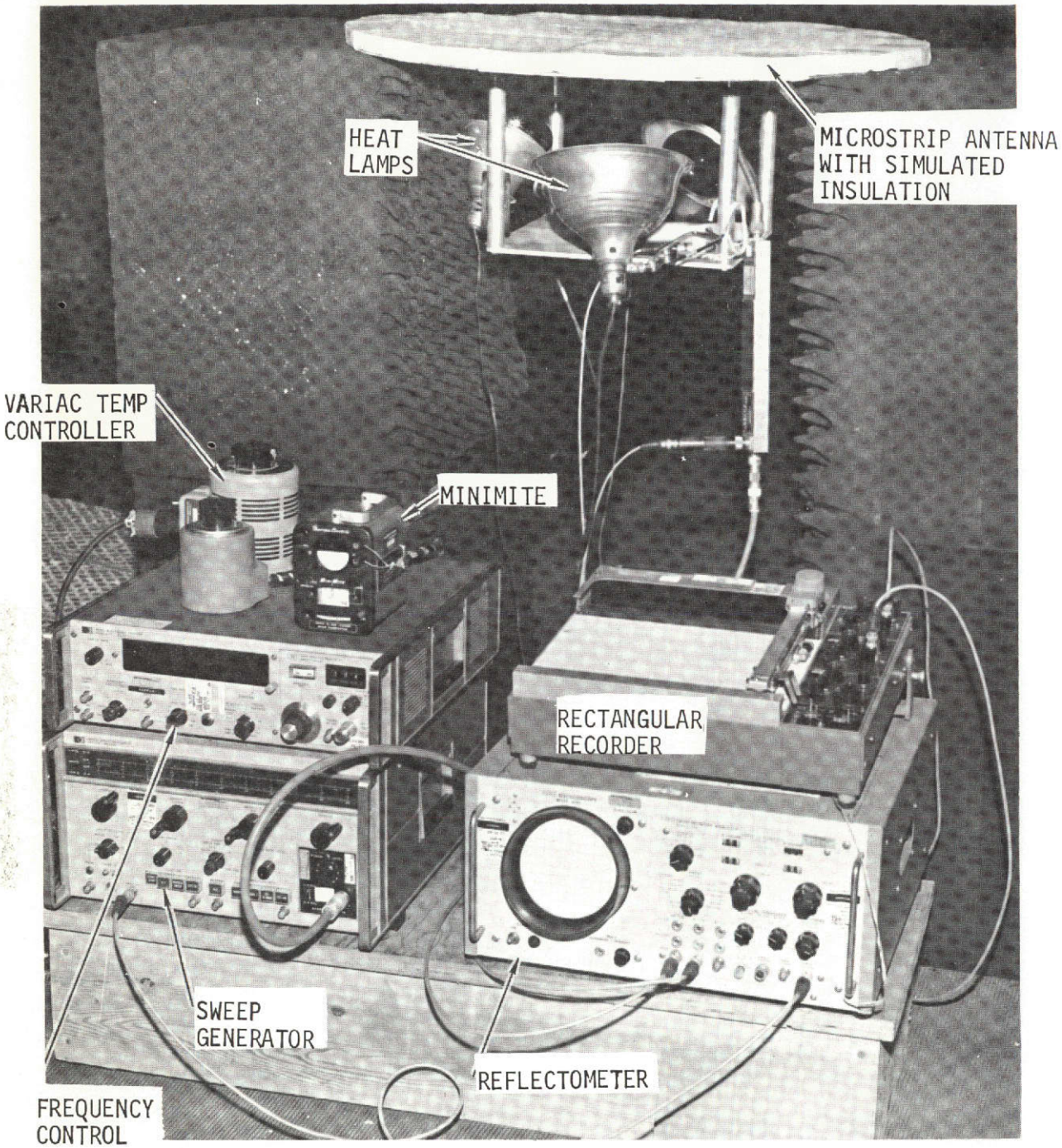


FIGURE 18
VSWR TEST SETUP

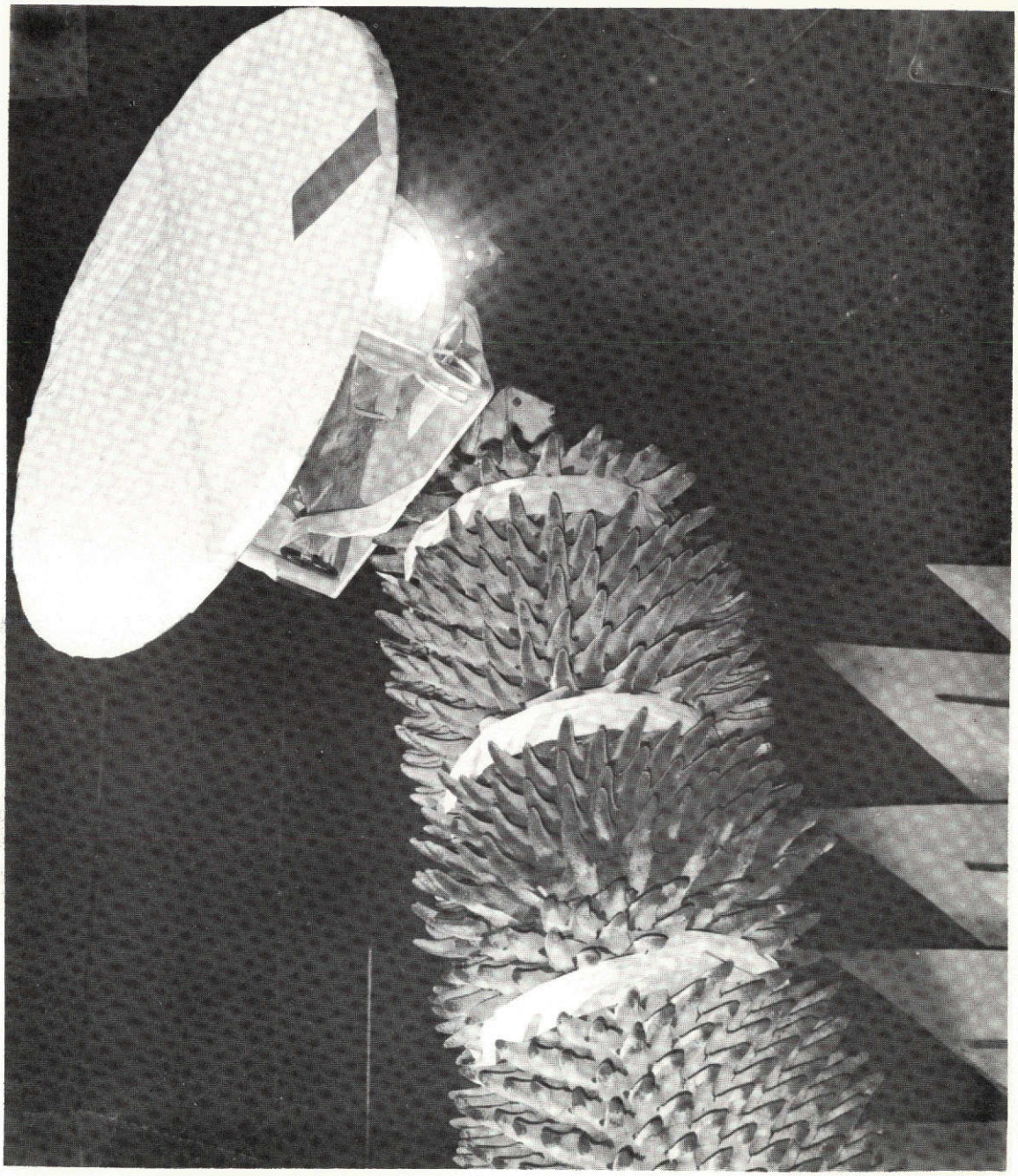

FIGURE 19
RADIATION PATTERN TEST SETUP

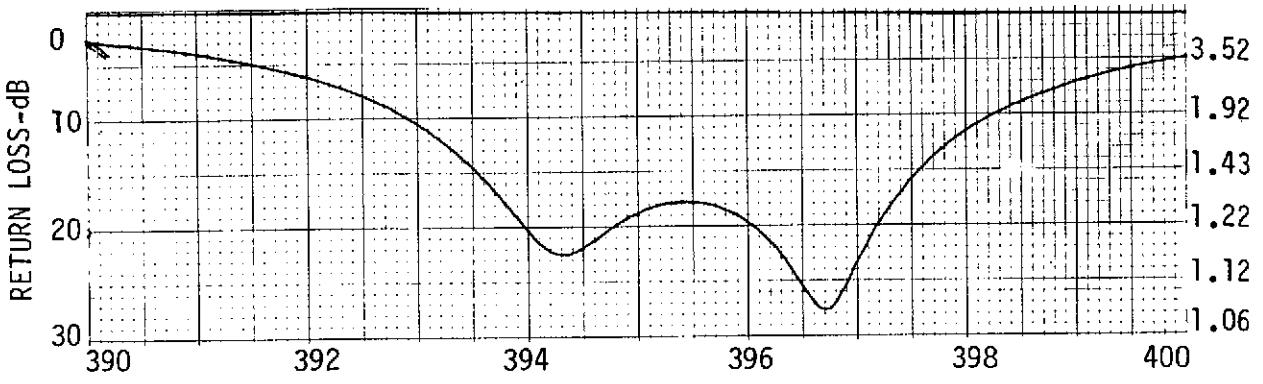


FIGURE 20

MICROSTRIP ANTENNA VSWR WITHOUT SIMULATED INSULATION

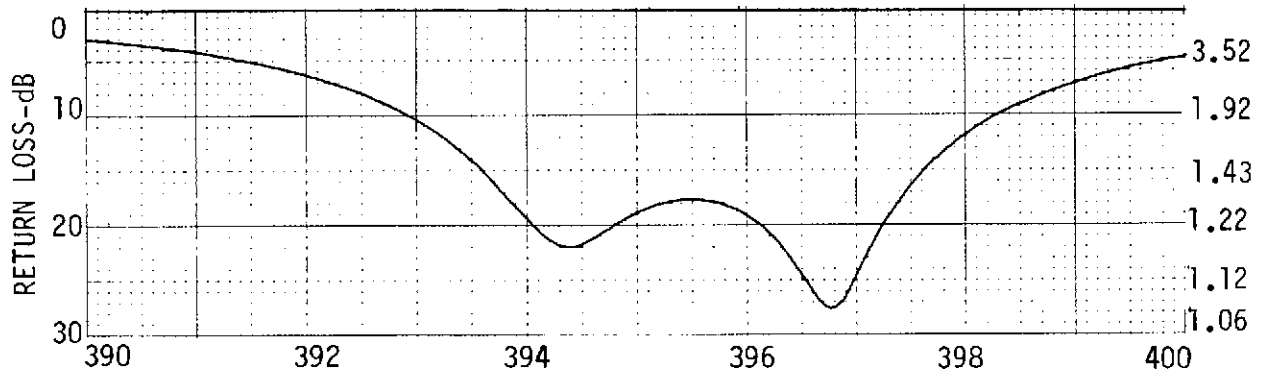


FIGURE 21

MICROSTRIP ANTENNA VSWR WITH SIMULATED INSULATION

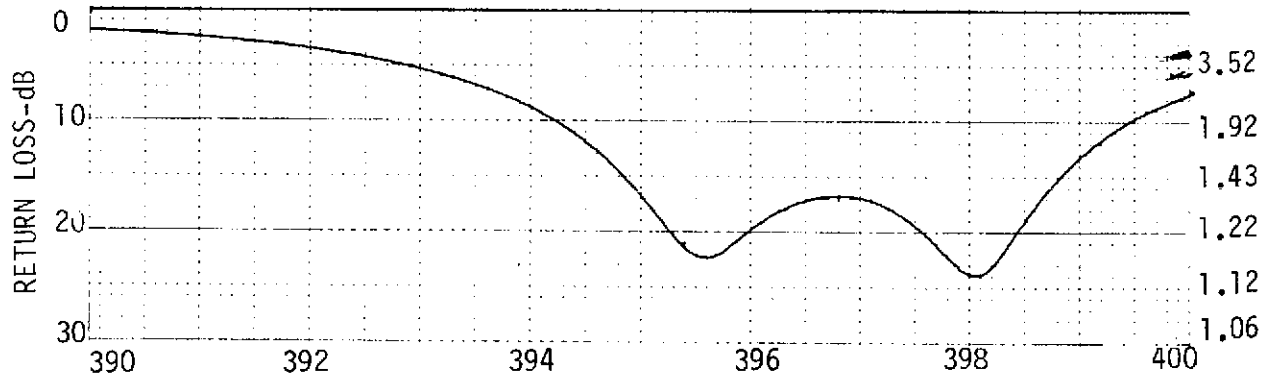


FIGURE 22

MICROSTRIP ANTENNA VSWR AT 344°K (160°F)

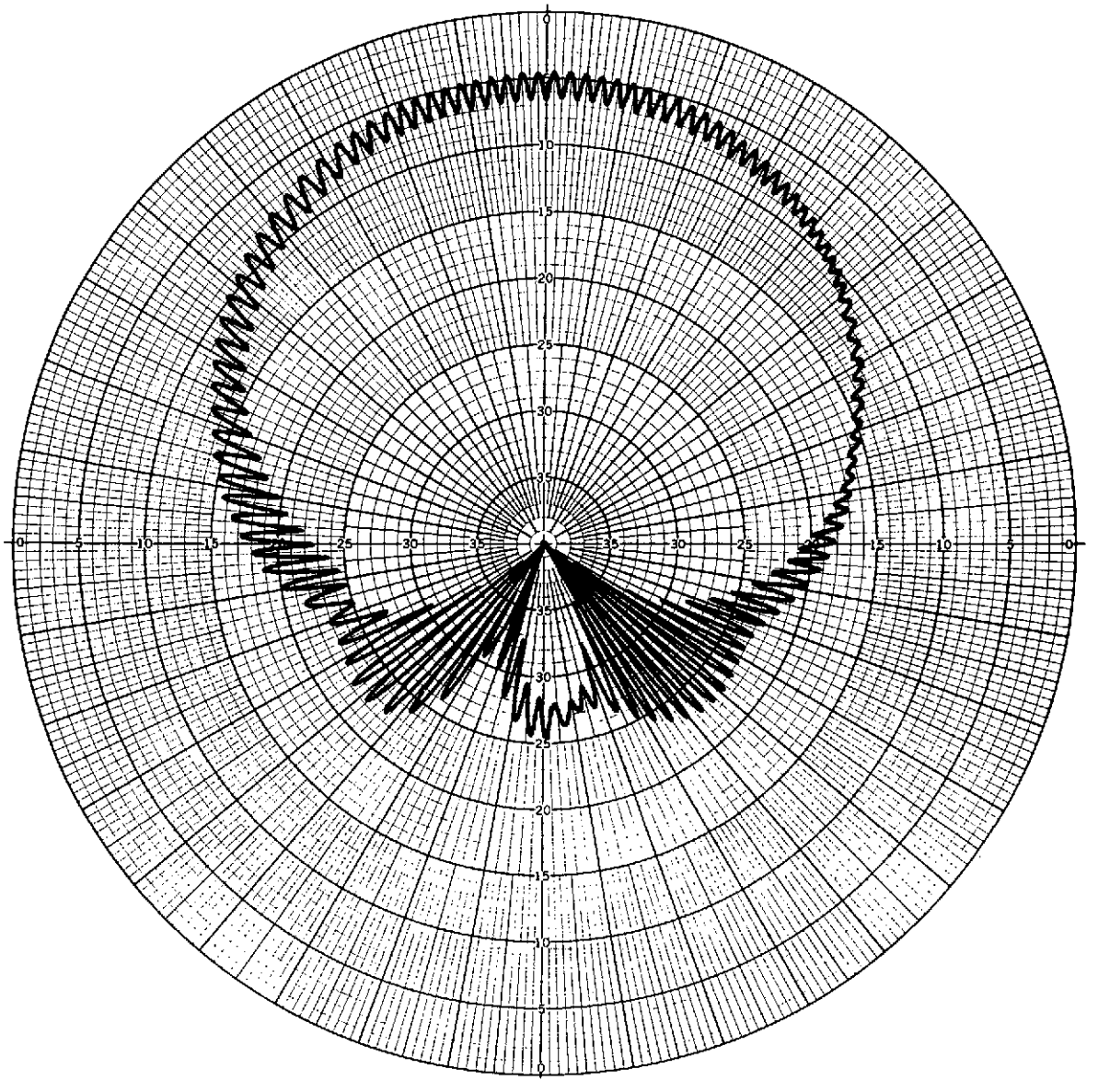


FIGURE 23
MICROSTRIP ANTENNA PATTERNS WITH SIMULATED INSULATION (ROOM TEMPERATURE)

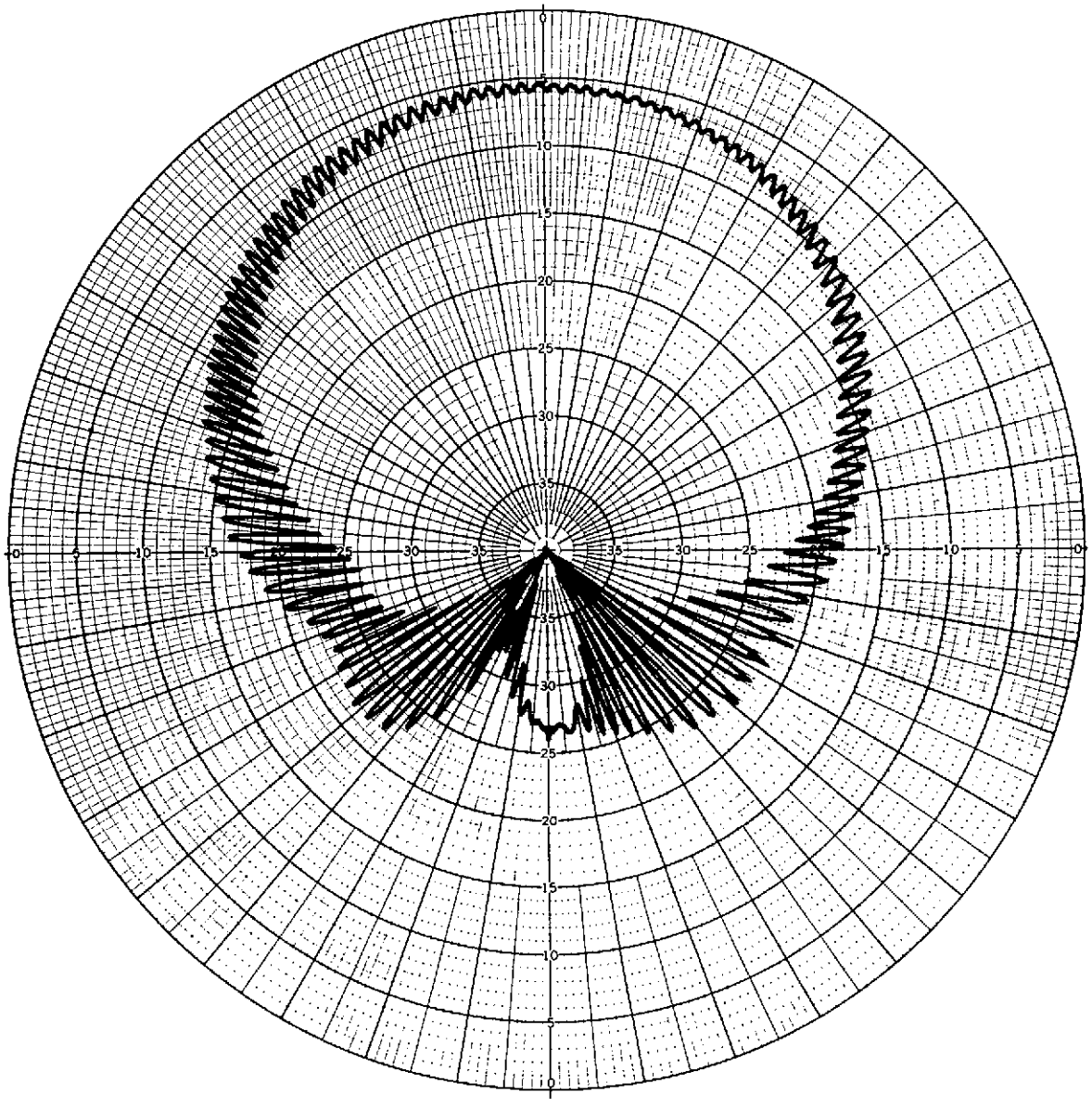


FREQUENCY = 395.50 MHz

FIGURE 23 (CONTINUED)
MICROSTRIP ANTENNA PATTERNS WITH SIMULATED INSULATION (ROOM TEMPERATURE)

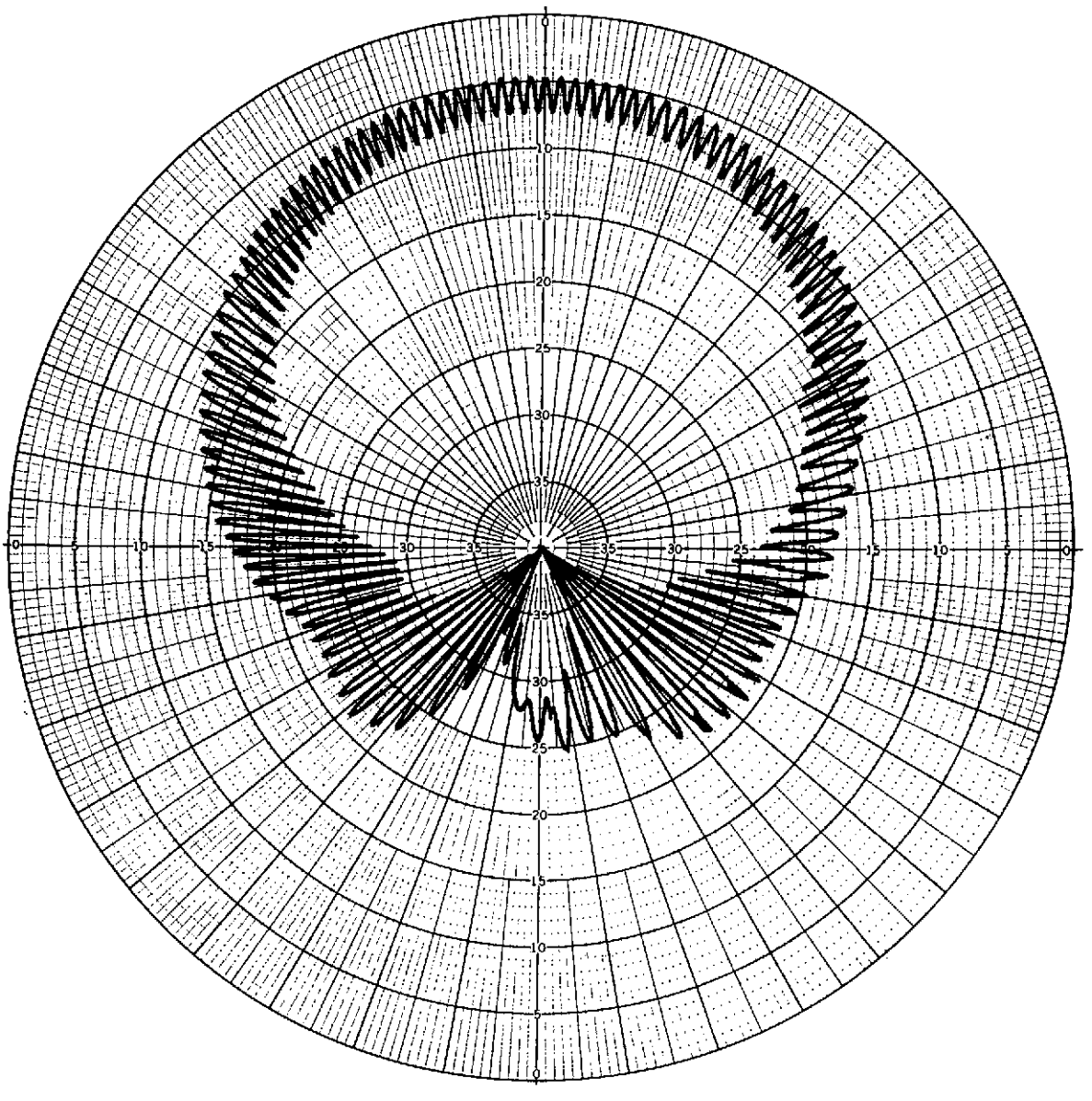


FIGURE 23 (CONCLUDED)
MICROSTRIP ANTENNA PATTERNS WITH SIMULATED INSULATION (ROOM TEMPERATURE)

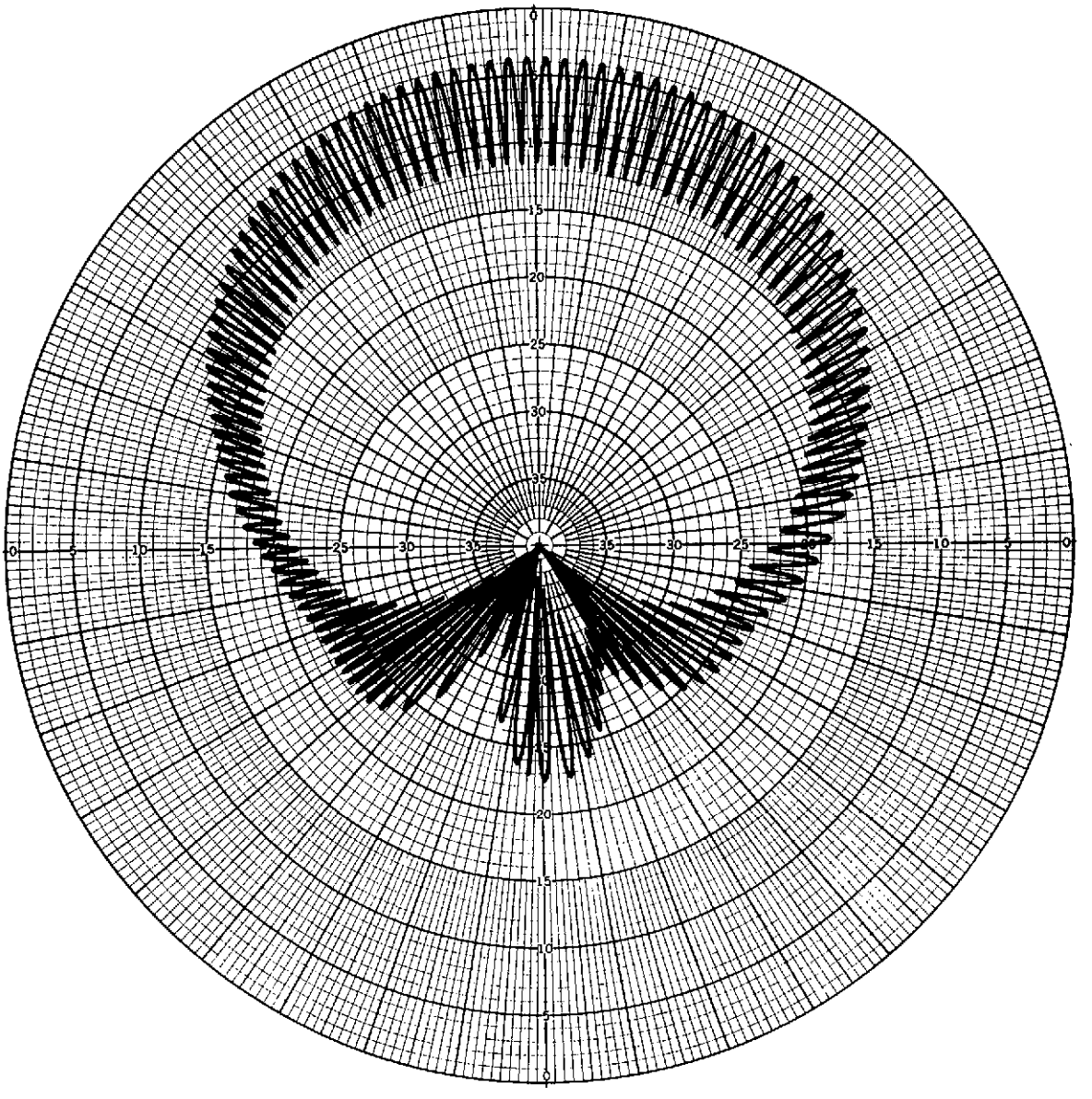


FREQUENCY = 395.11 MHz

FIGURE 24
MICROSTRIP ANTENNA PATTERNS WITH SIMULATED INSULATION (344°K(160°F))

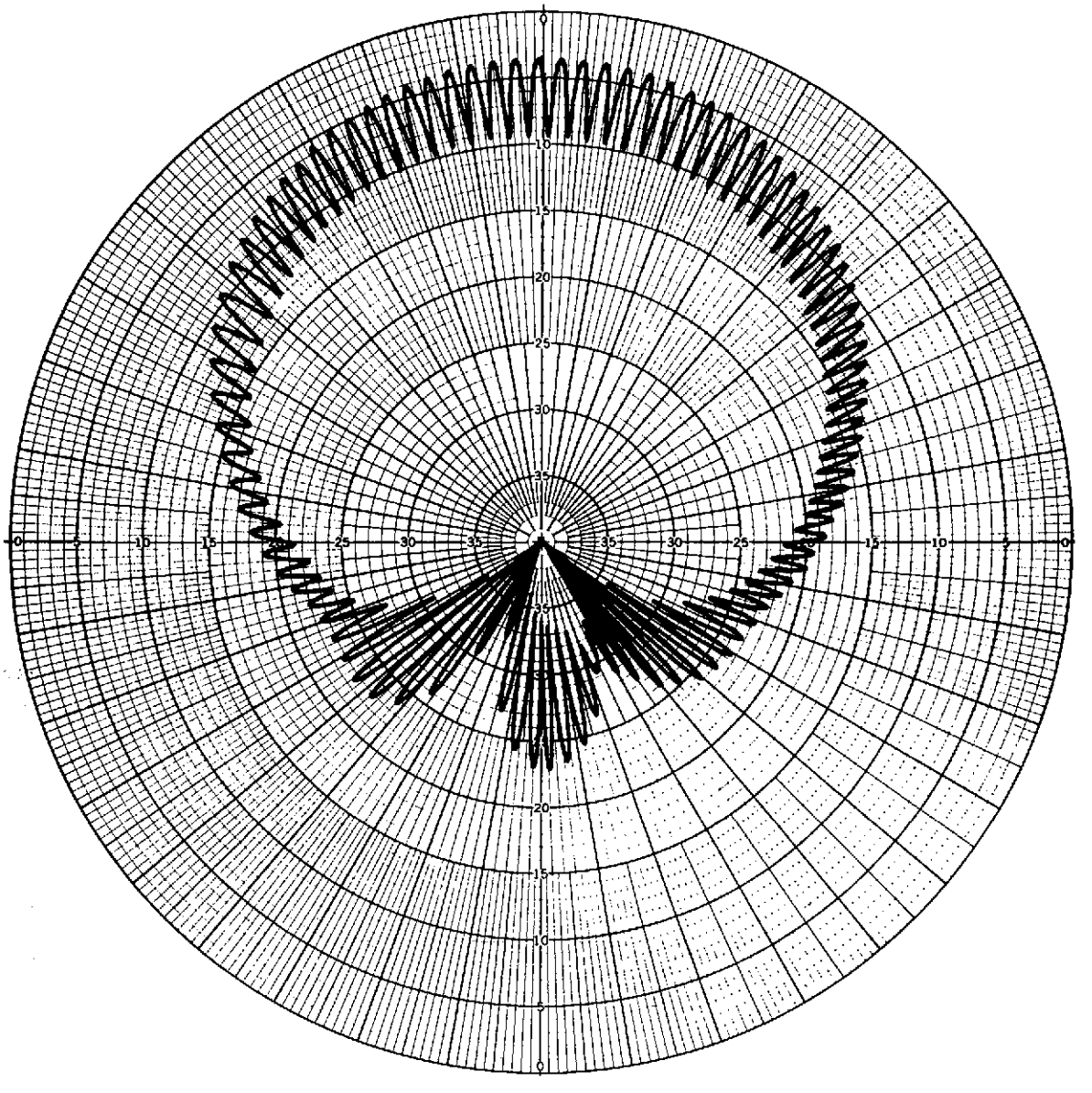


FREQUENCY = 395.50 MHz

FIGURE 24 (CONTINUED)
MICROSTRIP ANTENNA PATTERNS WITH SIMULATED INSULATION (344°K(160°F))

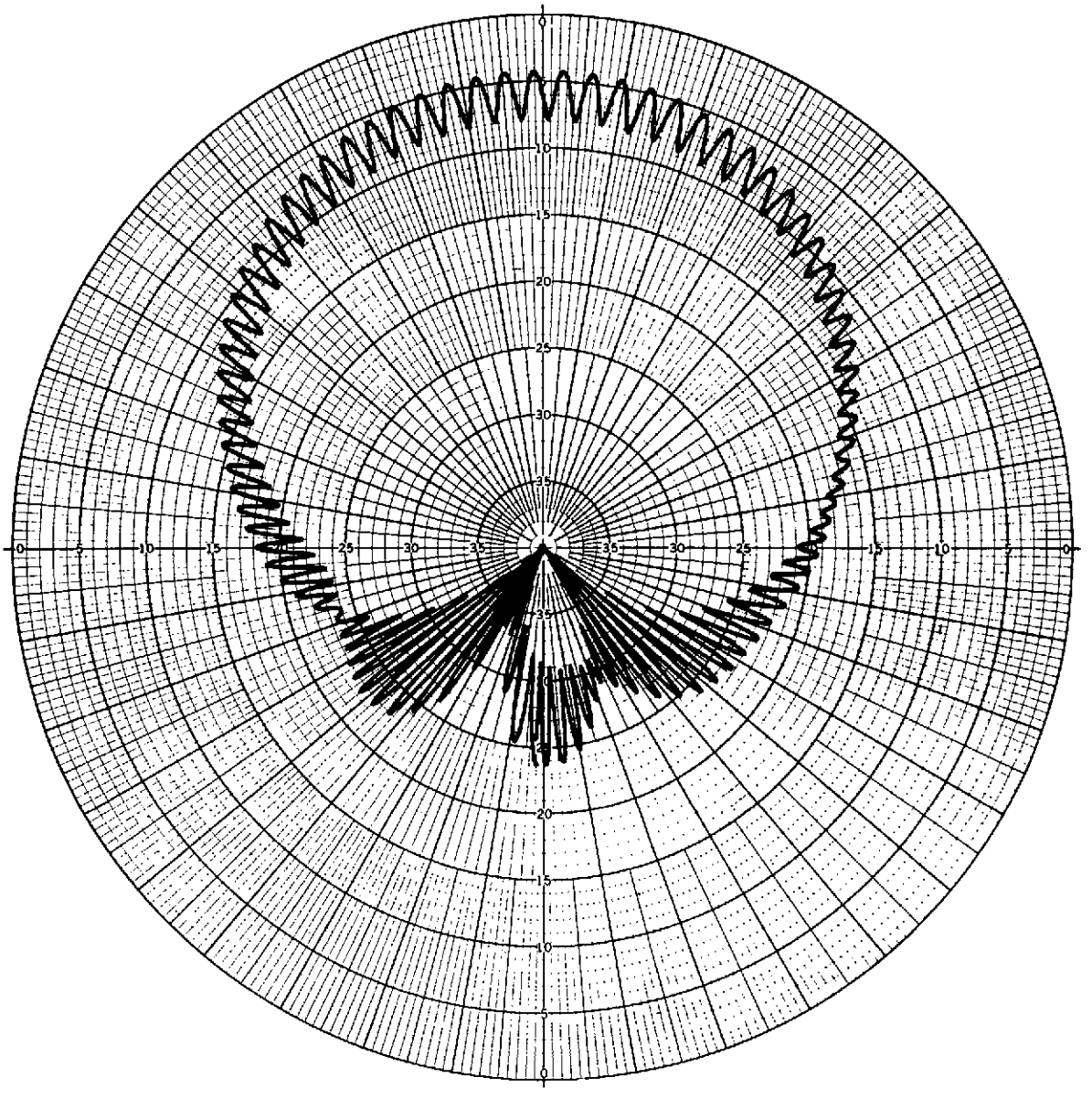


FREQUENCY = 395.92 MHz

FIGURE 24 (CONCLUDED)
MICROSTRIP ANTENNA PATTERNS WITH SIMULATED INSULATION (344°K(160°F))

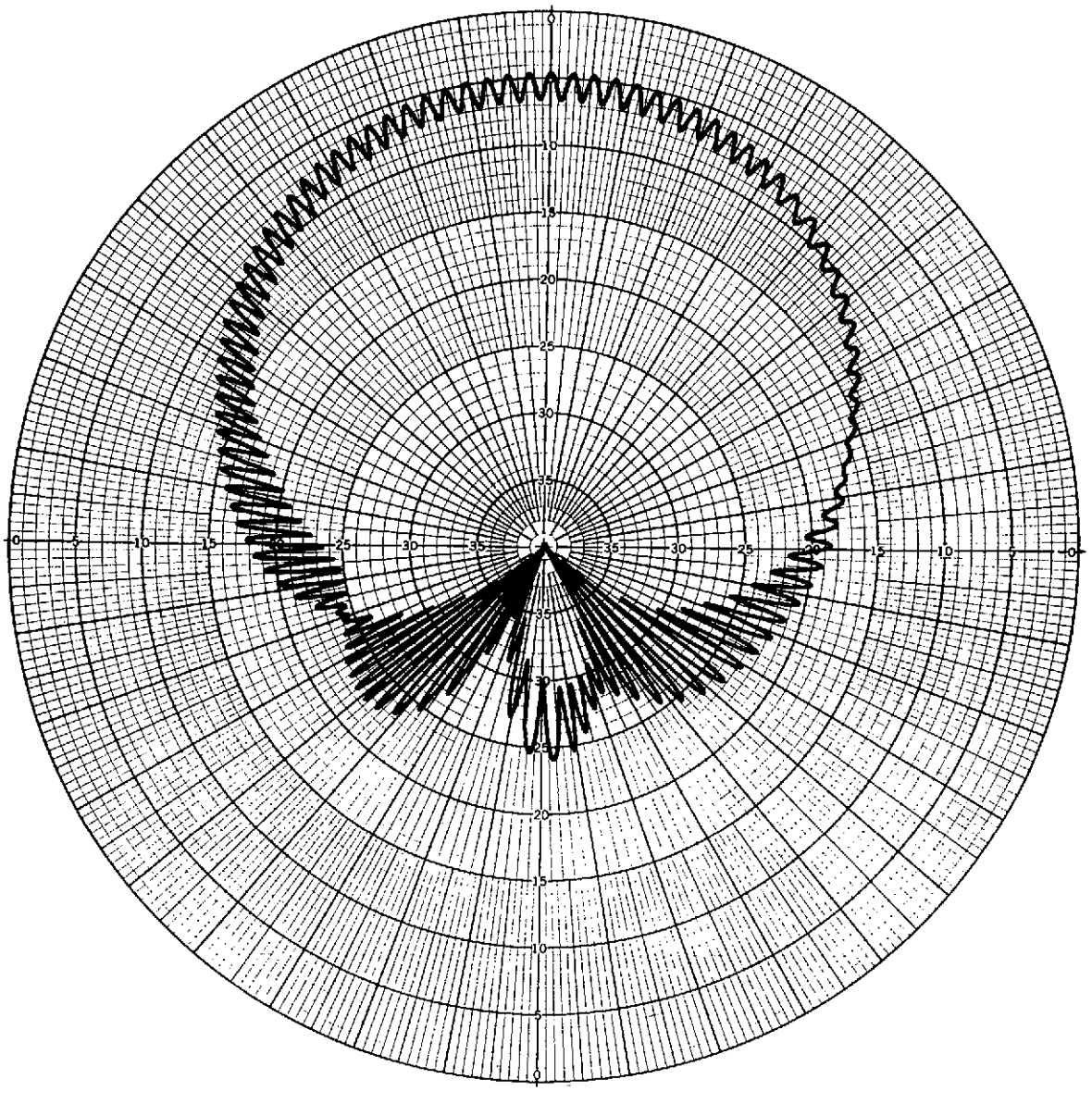

FREQUENCY = 396.25 MHz

FIGURE 25
MICROSTRIP ANTENNA PATTERNS WITH SIMULATED INSULATION (344°K(160°F)) ABOUT INCREASED RESONANT FREQUENCY

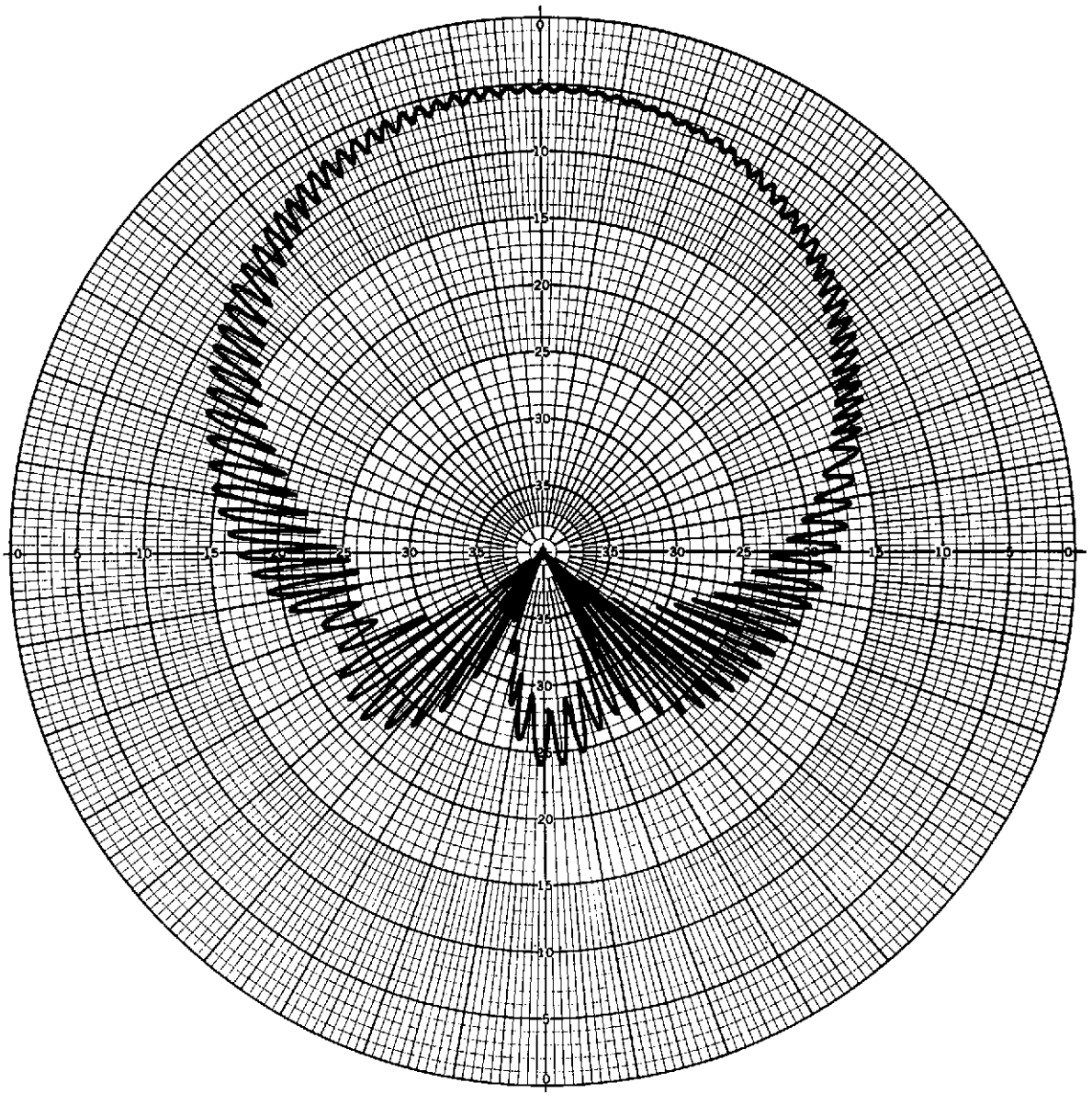

FREQUENCY = 396.65 MHz

FIGURE 25 (CONTINUED)
MICROSTRIP ANTENNA PATTERNS WITH SIMULATED INSULATION (344°K(160°F)) ABOUT INCREASED RESONANT FREQUENCY

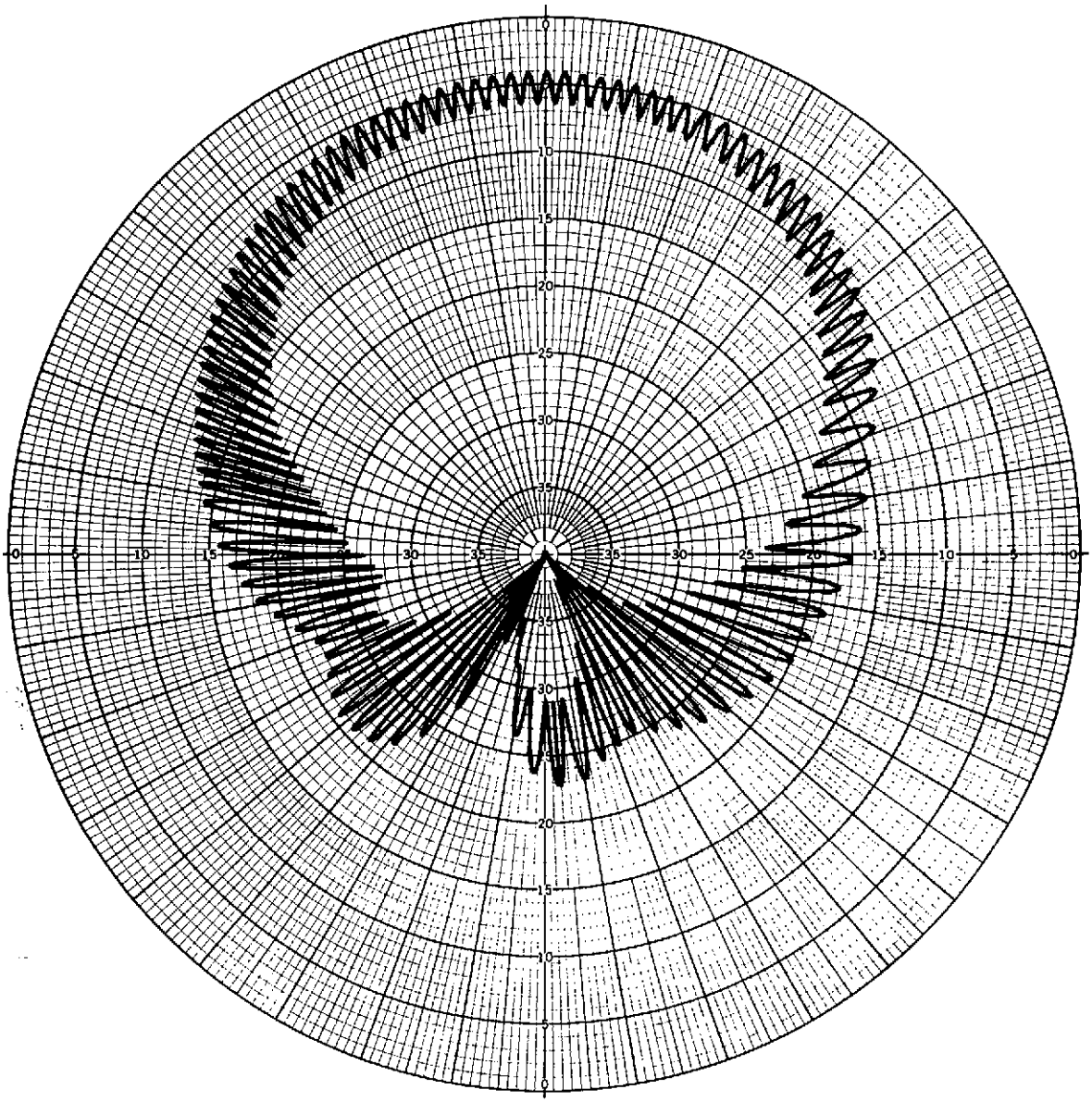

FREQUENCY = 397.05 MHz

FIGURE 25 (CONCLUDED)
MICROSTRIP ANTENNA PATTERNS WITH SIMULATED INSULATION (344°K(160°F)) ABOUT INCREASED RESONANT FREQUENCY

(a)
WITHOUT
INSULATION

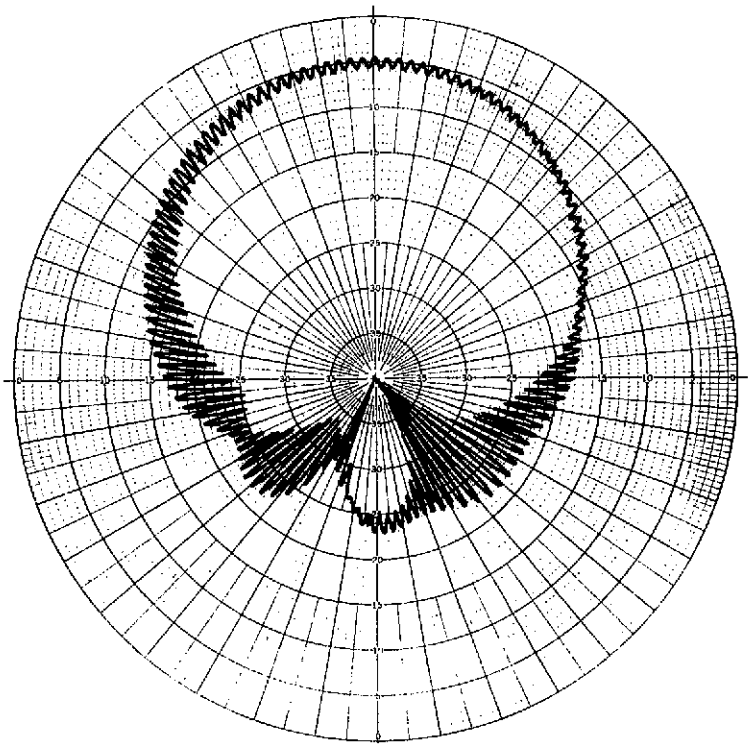

(b)
WITH
INSULATION

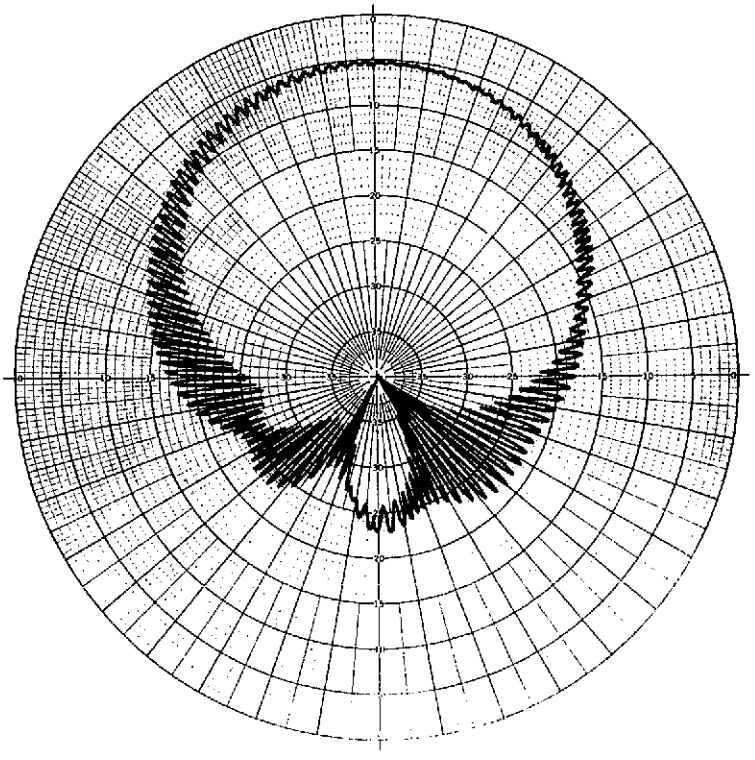

FIGURE 26

EFFECT OF SIMULATED INSULATION ON MICROSTRIP ANTENNA PATTERN (395.5 MHz)

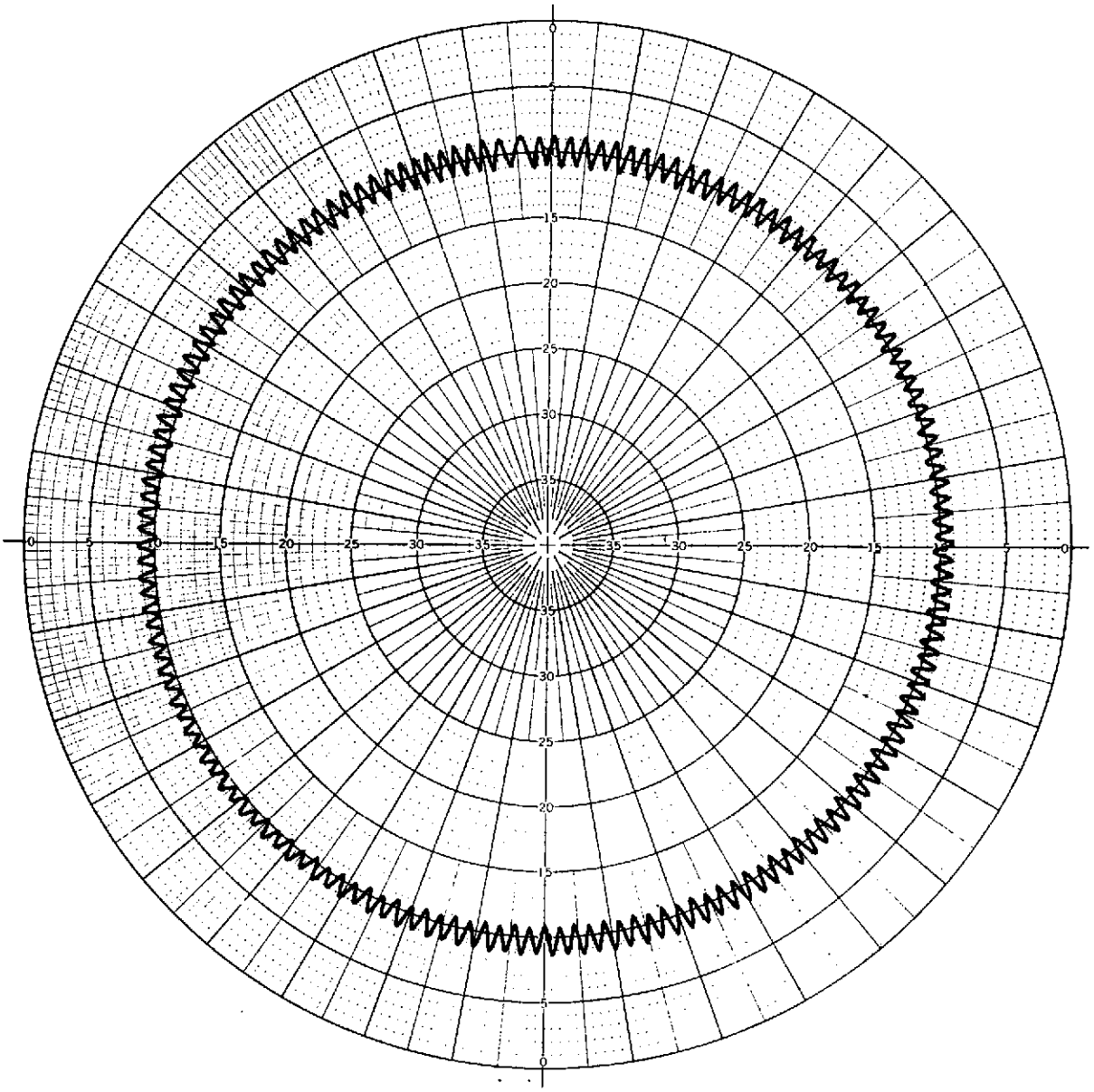


FIGURE 27
TYPICAL SYMMETRY OF A CIRCULAR MICROSTRIP ANTENNA (45° OFF ANTENNA NORMAL)

# APPENDIX I

## MICROSTRIP ANTENNA CHARACTERISTICS

## RESULTS FROM J. Q. HOWELL PAPER (REFERENCE 3)

| ANTENNA ELEMENT SHAPE AND DIMENSIONS (CM) | DIELECTRIC THICKNESS (CM) | DIELECTRIC CONSTANT | CALCULATED RESONANT FREQUENCY (GHz) | MEASURED RESONANT FREQUENCY (GHz) | BANDWIDTH VSWR = 3:1 (PERCENT) |
|---|---|---|---|---|---|
| SQUARE (2.54 x 2.54) | 0.079 | 2.59 | 3.67 | 3.57 | 1.7 |
| RECTANGULAR (2.54 x 5.08) | 0.079 | 2.59 | 3.67 | 3.57 | 2.4 |
| ROUND (r** = 1.27) | 0.079 | 2.59 | 4.29 | 4.07 | |
| SQUARE (2.97 x 2.97) | 0.159 | 8.5 | 1.74 | 1.71 | 1.0 |
| RECTANGULAR (0.958 x 0.762) | 0.064 | 10.3 | 6.13 | 6.04 | |
| SQUARE (0.958 x 0.958) | 0.064 | 10.3 | 4.88 | 4.78 | .9 |
| ROUND* (r = 3.493) | 0.318 | 2.5 | 1.58 | 1.51 | 3.5 |
| ROUND* (r = 3.493) | 0.159 | 2.5 | 1.58 | 1.57 | 1.8 |
| ROUND* (r = 13.890) | 1.270 | 2.7 | .387 | .378 | 3.2 |

* FED THROUGH GROUNDPLANE FROM THE BACK.
** r IS THE RADIUS

APPENDIX II
(REPRINTED BY PERMISSION OF IEEE FROM IEEE TRANSACTIONS ON ANTENNAS AND PROPAGATION JANUARY 1974, VOLUME AP-22, NUMBER 1 PAGES 74-78)





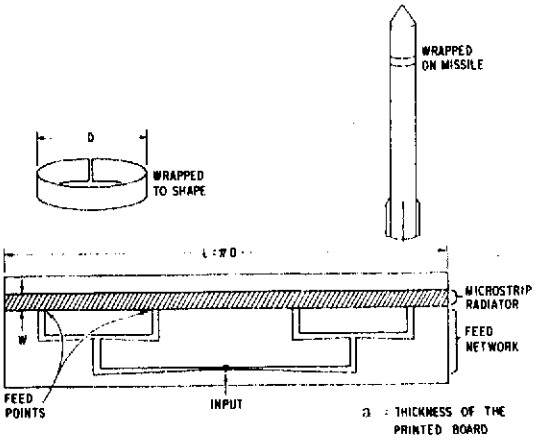


Fig. 1. Microstrip wraparound antenna.

# Conformal Microstrip Antennas and Microstrip Phased Arrays

ROBERT E. MUNSON

***Abstract*—A new class of antennas using microstrips to form the feed networks and radiators is presented in this communication. These antennas have four distinct advantages: 1) cost, 2) performance, 3) ease of installation, and 4) the low profile conformal design. The application of these antennas is limited to small bandwidths. Phased arrays using these techniques are also discussed.**

## I. Introduction

High-velocity aircraft, missiles, and rockets require conformal, thin antennas. Ideally, an antenna "paper thin" would best suit the aerodynamic and mechanical engineer. This antenna would neither disturb the aerodynamic flow, nor would it protrude inwardly to disrupt the mechanical structure.

With a microstrip (a single side etched) printed circuit board antenna, the two aforementioned goals are nearly attained. In addition, the desire for a lower cost antenna can be met because the single printed circuit (PC) board (microstrip) antenna is manufactured with the same low cost photo-etch processes used to make electronic printed circuit boards. The single board is photo etched on one side only (no front-to-back registration is required); no board alignments are required.

The microstrip phased array to be discussed is an antenna incorporating the basic radiating aperture with its associated microwave feed system all printed on the outside of a printed circuit board. It is a new microstrip device[1] that includes an efficient electrically thin microstrip radiator and integrated feed network, matching network, phasing network, switching network, and filter network, if required.

Currently, solid-state components are also added directly to this board to provide oscillators, amplifiers, phase shifters, switches, and receivers. It would appear that the feed lines would interfere with the radiation but they do not because they are electrically close to the ground plane which is the back of the antenna, and because the feed lines are perpendicular to the electric field being emitted by the radiator, i.e., a metal septum perpendicular to the electric field.

Manuscript received April 4, 1973; revised September 5, 1973.
The author is with the Ball Brothers Research Corporation, Boulder, Colo. 80302.
[1] Patent #3 713 162 "Single slot cavity antenna assembly," dated Jan. 23, 1973.

This communication will discuss microstrip arrays of three general types: wraparound microstrip antennas that wrap around missiles, rockets, and satellites to provide omnidirectional coverage; flat thin microstrip antennas that provide a high gain fan beam or a pencil beam; a phased array that consists of flat (or curved) thin microstrip antennas with pin diodes added to the microstrip substrate to provide an electronic beam steering capability.

## II. Microstrip Wraparound Antennas

The wraparound antennas which provide omnidirectional coverage are similar in performance (coverage and bandwidth) to the stripline (two layer PC board) antennas discussed by Waterman and Henry [1], Campbell [2], and Johnson [3]. In general, stripline and microstrip antennas will produce bandwidths (VSWR $< 2:1$) of 30 MHz to 100 MHz in the $L$ band and $S$ band regions with a 1- to 2-dB variation in the roll plane. The microstrip wraparound antenna consists of two parts: 1) microstrip feed network and 2) microstrip radiator.

## III. Microstrip Feed Network

The microstrip feed network (Fig. 1) is a parallel (corporate) feed network where two-way power splits and equal line lengths result in equal power and equal phase to all of the feed points. The number of power divisions can be 2, 4, 8, 16, etc. The number of feeds, power divisions, required is dictated by the microstrip radiator. The number of feed points $N_F$ must exceed the number of wavelengths in the dielectric in the $L$ direction: $N_F > L_D$; $L_D$ is the number of wavelengths in the dielectric $= L_{(\epsilon_r)^{1/2}}/\lambda_0$; $\epsilon_r$ is the relative dielectric constant of the board material being used; $\epsilon_r = 2.45$ is typical; if only the TEM mode is to be excited. This mode will in turn excite only $TM_{0M}$ modes in free space (no roll pattern variation). If $N_F < L_D$, then higher order modes will be excited on the microstrip radiator. These modes will excite $TM_{xM}$ modes in free space [4, p. 276]. The excitation of higher order modes on the microstrip radiator will result in breakup of the roll (xz) plane patterns. As an example, the number of feeds required for an $S$ band 2290 MHz ($\lambda_0 = 12.7$ cm) wraparound for a 25.4-cm missile would be

$$L = \pi D = 79.756 \text{ cm}$$

$$L_D = \frac{L_{(\epsilon_r)^{1/2}}}{\lambda_0} = \frac{79.756(2.45)^{1/2}}{12.7} = \frac{79.057 \cdot 1.6}{12.7} = 10.05$$

$N_F > 10.05$ and $N_F$ can be 2, 4, 8, 16, 32, 64, etc.

Thus $N_F$ must be 16.

Two types of feed network are used to accomplish a 2, 4, 8, 16, etc., power split. Most often tapered lines, Fig. 2 (a), are used to transform a 50-Ω impedance to 100 Ω, so that it can be combined in parallel with another 100-Ω line. The same procedure is shown in

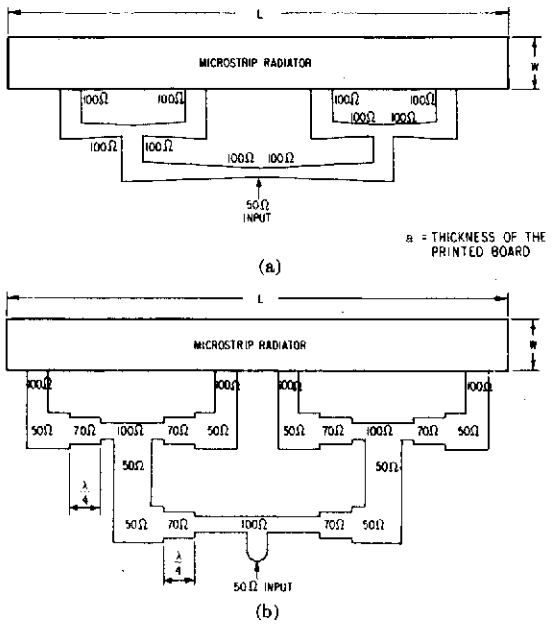


Fig. 2. (a) Tapered line parallel feed network. (b) Quarter-wave transformer parallel feed network.

Fig. 2(b) for a quarter-wave transformer technique. The impedance of the quarter-wave transformer is given by

$$Z_{\text{transformer}} = (Z_{\text{in}} \times Z_{\text{out}})^{1/2} = (100 \cdot 50)^{1/2} \approx 70\Omega.$$

The number of feed points possible for a very long radiator is limited only by the allowable system losses that can be allocated to the feed network. However, it is desirable to use the minimum $N_F$ satisfying the condition $N_F > L_D$. If 32 feeds were used instead of 16 the preceding example would result in input impedances exceeding 300 Ω which would be impossible to match efficiently with microstrip feed lines.

## IV. Microstrip Radiator

Two types of microstrip radiators are generally used: the long microstrip radiator and the patch radiator. The long microstrip radiator shown in Figs. 2(a) and (b) is shown in top and side view in Figs. 3(a) and (b), respectively. Gap $A$ is an infinitesimal slot (in 0.79 mm microstrip $a/\lambda \approx 1/150$ at $S$ band). The admittance of a slot radiator is given in Harrington [4, p. 183] for small $ka(a/\lambda < 0.1)$ which is always the case in microstrip antenna practice

$$G_a \approx \frac{\pi}{\lambda\eta}\left[1 - \frac{(ka)^2}{24}\right]$$

$$B_a \approx \frac{3.135 - 2\log ka}{\lambda\eta}.$$

In most microstrip applications $ka/24 \ll 1$ and the conductance simplifies to $G_a = \pi/\lambda\eta = 1/\lambda(120)$ mho/m or $R_a = 120\lambda$ Ω·m. The conductance is expressed in per unit length so that the resistance of the Slot $A$ in Figs. 3(a) and (b) is obtained by dividing $R_a$ by the length

$$r_a = \frac{R_a}{L} = \frac{120\lambda}{2\lambda} = 60\Omega.$$

The dielectric under the microstrip radiator can be treated as a transmission line approximately $\lambda/2$ long. The problem with the microstrip transmission line is its very low impedance, typically 1 to 10 Ω. This section of parallel-plate transmission line does transform the Slot $A$ impedance from 60 Ω through small inductances near the center and back to 60 Ω at Slot $B$ [see Fig. 3(c)]. At this

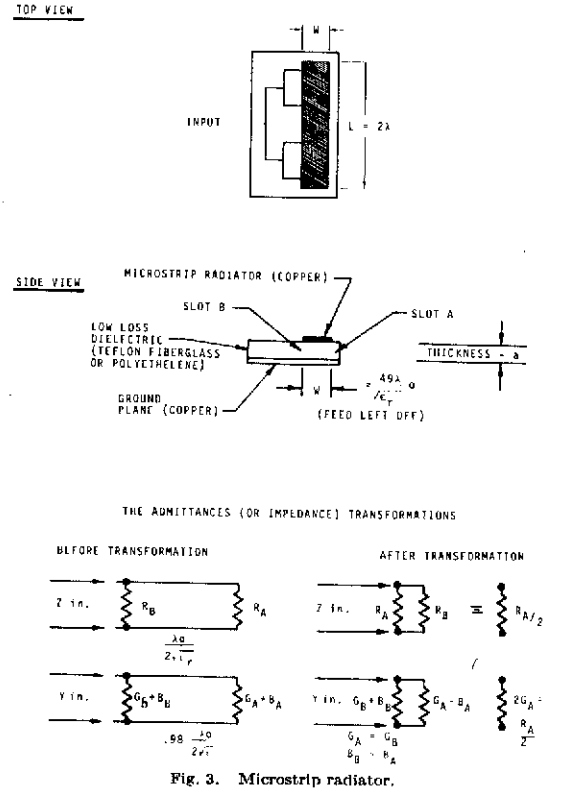


Fig. 3. Microstrip radiator.

point the two impedances combine in parallel to give

$$\frac{1}{r_{\text{in}}} = \frac{1}{r_a} + \frac{1}{r_b} = \frac{1}{60} + \frac{1}{60}$$

$$r_{\text{in}} = 30\ \Omega.$$

In the example shown in Fig. 3(a) this impedance is split between four feed points with each feed theoretically seeing 120 Ω. In practice, this is the measured impedance. This theory is very accurate in predicting the input impedances for many designs each with different frequencies, thicknesses, feed point separations, and number of feed points. The previous discussion did not treat the implications of the reactive component of the admittance $B_A$ because it does not affect the conductance component of admittance $G_A$. The effect of the reactance $B_A$ is to produce a resonance slightly short of a half-wavelength. For example, we can consider the admittance of Slot $A$ to be

$$Y_A = G_A + B_A.$$

At a distance of 0.5λ on the parallel-plate transmission line, the admittance has been transformed to $Y_A = G_A + B_A$ and these admittances combine directly in parallel with $Y_B$ to produce $Y_{\text{in}} = 2G_A + 2B$ which is not resonance. At a distance just short (usually 0.49λ to 0.48λ) of a half-wavelength in the parallel-plate transmission line transformer the transformed admittance of Slot $A$ is

$$\tilde{Y}_A = G_A - B_A$$

and at this length slightly short of a half-wavelength $[\lambda_0/2(\epsilon_r)^{1/2}]$ resonance is established with no susceptance

$$Y_{\text{in}} = G_A + G_B = 2G_A$$

$$Z_{\text{in}} = R_A/2$$

and for the example

$$Z_{\text{in}} = R_{\text{in}} = 30\ \Omega \text{ (total resistance)}$$

$$R_{\text{in}} = 120\ \Omega \text{ (per feed)}.$$

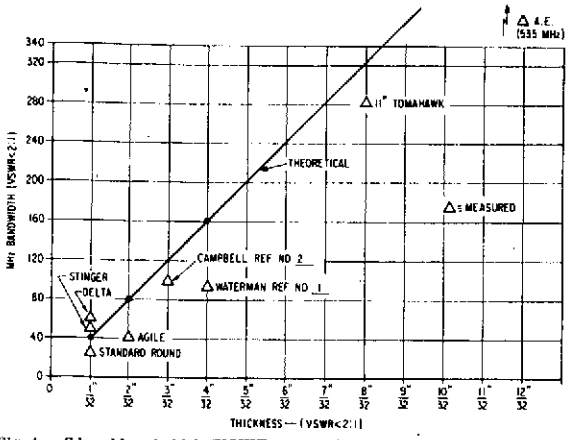


Fig. 4. *S* band bandwidth (VSWR 2–1) as function of antenna thickness.

The bandwidth of a microstrip antenna is dominated by the microstrip parallel-plate transmission line between Slot *A* and *B*. Since the transmission line usually has an impedance close to 1 Ω and the two slots have impedances close to 100 Ω, the transformation exists usually for 1-percent bandwidth for VSWR < 2:1. The bandwidth can be easily calculated by adding

$$Y_{in} = \bar{Y}_A + Y_B$$

(where the amount that $Y_A$ is transformed depends upon frequency.), and then evaluating the two frequency points at which the reactances cause the VSWR to equal 2:1. Several measured bandwidths of microstrip phased arrays are shown in Fig. 4 in conjunction with the theoretical bandwidth as calculated earlier.

The major limitation of the microstrip antenna is the bandwidth. To substantially increase the bandwidth of microstrip antennas requires an increase of the thickness of the parallel plate transformer which increases the characteristic impedance of the transformer. This increase in thickness is undesirable if the antenna is to remain low profile and conformal. In most applications the advantages of a low profile antenna outweighs the disadvantage of its narrow bandwidth because present applications require less than 1 percent. Three other methods of increasing the bandwidth are currently being investigated: 1) use of a high ($\epsilon_r$) dielectric constant to decrease the cavity length; 2) increasing the inductance of the microstrip radiator by cutting holes or slots into it. Experiments show increased bandwidth but at the cost of efficiency, in fact the same increase could have been attained by using a more lossy substrate; 3) broadbanding by addition of reactive components as discussed in Jasik [5] to reduce VSWR across a limited bandwidth. This technique is very limited usually to 50 percent of $\Delta f_0/f_0$.

## V. Microstrip Antenna Pattern Coverage for Omniapplications

The pattern coverage for the omniantenna shown in Fig. 1 depends on the diameter of the missile. The limiting factor in omnidirectional pattern coverage is a singular hole at the tip and tail of the missile which gets *narrower* as the diameter of the missile *increases*. For instance, a 15-in diameter antenna produces a null along the missile axis of radius 1° at the −8-dB gain level. The fraction area with gain below −8 dB is given by

$$F_N = \left(\int_{0^\circ}^{360^\circ}\int_{0^\circ}^{1^\circ} \sin\theta\, d\theta\, d\phi + \int_{0^\circ}^{360^\circ}\int_{179^\circ}^{180^\circ} \sin\theta\, d\theta\, d\phi\right) \Big/ \int_{0^\circ}^{360^\circ}\int_{0^\circ}^{180^\circ} \sin\theta\, d\theta\, d\phi$$

$$\approx 0.0002.$$

Conversely, the fraction of the area with gain above −8 dB is 0.9998, or 99.98 percent coverage with gain greater than −8 dB. The percent coverage increases without limit for larger diameters until a nearly perfect coverage is attained for a single linear polarization.

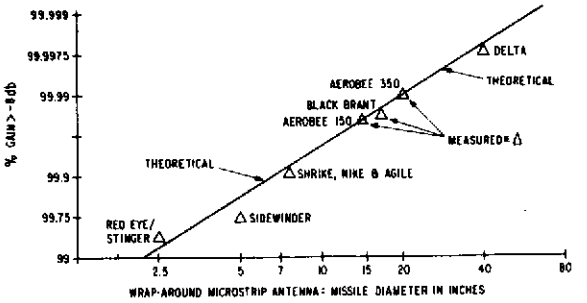


Fig. 5. Pattern coverage versus diameter for microstrip wraparound antennas on smooth cylinders.

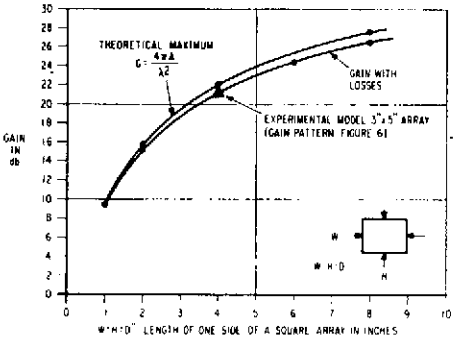


Fig. 6. Gain versus size for flat microstrip arrays (frequency is *X* band or 10 GHz and $\lambda_0 = 1.18''$).

The percent coverage is only a function of diameter and is independent of antenna thickness. The theoretical and experimental pattern coverages for microstrip antennas on a smooth cylinder are given in Fig. 5 for gain greater than −8 dB.

## IV. Flat-Plate Microstrip Antennas

Unwrapping omniwraparound antennas and mounting them flat on a metal surface or in free space produces a high gain fan beam antenna pattern. By arraying several antennas side by side, a pencil beam is produced. Theoretically, the microstrip radiators produce a uniform illumination of the aperture and the gain of a uniformly illuminated aperture is given by Silver [6] as

$$G_a = \frac{4\pi A}{\lambda^2}.$$

In practice, the microstrip feed line attenuation subtracts from this gain

$$G_{actual} = 10\log\left(\frac{4\pi A}{\lambda^2}\right) - \alpha$$

$$\alpha_{line} = \alpha L.$$

The attenuation is dependent on frequency and line length. At *X* band a microstrip line on 0.79-mm board has an attenuation $\alpha = 0.047$ dB/cm. The length of the microstrip feed line for a given array is half of the height plus half of the width of the array

$$L = \frac{W}{2} + \frac{H}{2}$$

therefore

$$\alpha = (\alpha/2)(W + H)$$

at *X* band for a 12.7-cm × 7.62-cm antenna $\alpha_{line} = 0.48$ dB. Gain as a function of size for a square microstrip array is shown in Fig. 6.

Fig. 7. High gain flat microstrip antenna.

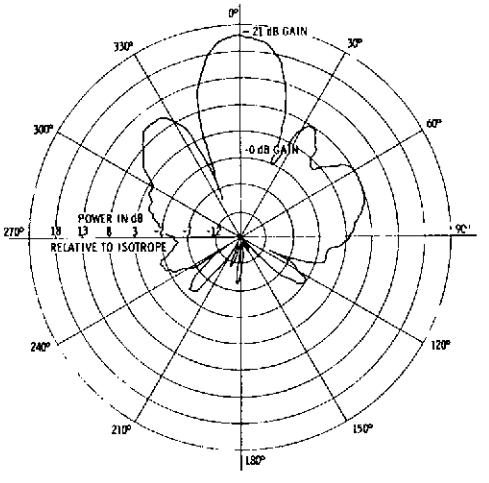


Fig. 8. Gain and pattern of 7.62 cm x 12.7 cm x 0.79 cm microstrip array at 9.92 GHz.

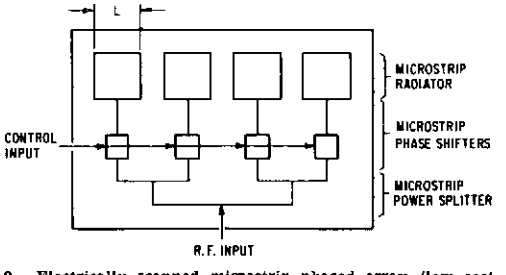


Fig. 9. Electrically scanned microstrip phased array (low cost and low profile).

An experimental model 7.62 cm × 12.7 cm × 0.79 mm (Fig. 7) was built and tested and confirms a gain (Fig. 8) in agreement with the theoretical predictions (Fig. 6). The measured gain of 21 dB is also plotted on the predicted gain curve (Fig. 6). The microstrip antenna offers high gain for a low cost. It also offers a low profile antenna that can operate flush mounted to a metal surface.

## VII. Microstrip Phased Arrays

By adding "pin diodes" for digital phase shifting, Fig. 9, to the microstrip substrate an integrated electrically scanned antenna is attained. The process of phasing the radiators to scan the beam requires breaking up the microstrip radiators into individual elements. The individual microstrip elements (a sample is shown in Fig. 10) work just like the long microstrip radiator described in the previous section. By using $L$ the length of the individual microstrip radiators we can calculate the resonant length, input impedance, and bandwidth of the microstrip radiator just as was done in the previous section.

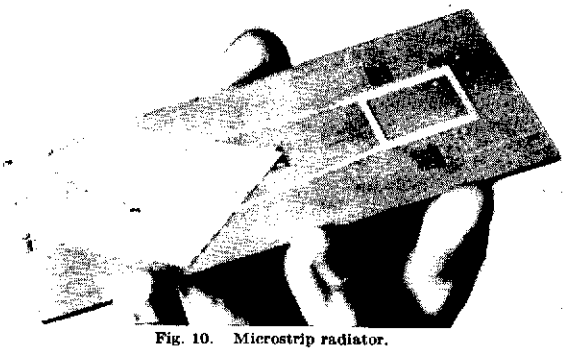

Fig. 10. Microstrip radiator.

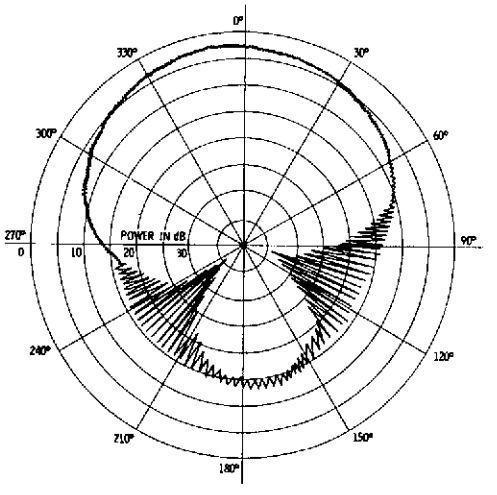


Fig. 11. Radiation pattern of microstrip patch. Patterns were measured with spinning dipole to demonstrate low axial ratios to wide angle.

This works quite well except when the $L$ of the individual radiator is not reduced below 0.25 $\lambda_0$. For $L < 0.25\ \lambda_0$ the radiation resistance of the microstrip radiator rapidly disappears, i.e., the slots $A$ and $B$ are not long enough to match free-space efficiently because their size has been reduced below cutoff for the modes that must be matched to free space as described by Harrington [4, p. 278].

Each of these microstrip radiators are rectangular microstrip elements and each one produces a hemispherical coverage pattern, Fig. 11. A conceptual model of the phased array shown in Fig. 9 was built and tested to demonstrate a complete microstrip electrically scanned phased array. The patterns scanned to the angles predicted with a gain within 1 dB of the expected gain, Fig. 12. The phase shifters used were microstrip 90° hybrid phase shifters with diodes in the two output legs. Driving two diodes in the two output legs of the hybrid changes the phase of the reflected power in the reflected port of the hybrid. The phase shift attained is twice the distance the short reference is moved in the two output legs. Three phase shifters were used in series for each element to produce 0°, 45°, 90°, 135°, 180°, 225°, 270°, or 315° phasing of each element. The phase shifters along with all of their dc feed lines, dc blocks, RF blocks, the RF corporate feed network, the matching network, and the microstrip radiators were all photo etched on one side of one microstrip board.

## VIII. Conclusions

Microstrip antennas constitute a new class of onmidirectional antenna for missiles and satellites. These antennas are capable of producing a predictable and nearly perfect onmidirectional coverage. A new low cost low profile flat microstrip array is shown to have 90-percent aperture efficiency. In addition, the flat microstrip

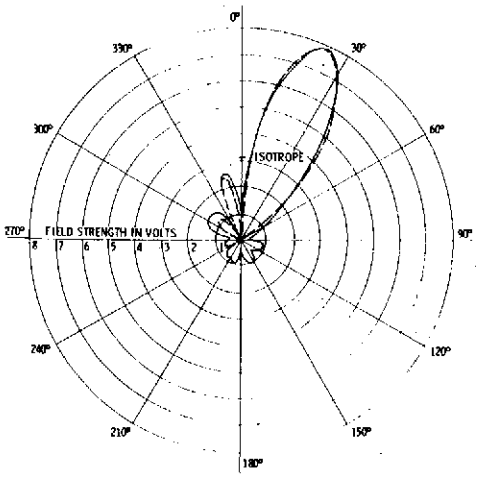


Fig. 12. Electronically scanned 4 element array. — measured pattern. --- predicted pattern.

arrays can be electronically scanned with the addition of phase shifters.

These antennas are inexpensive to fabricate because of the photo etch process used in their manufacture, and inexpensive to install because they are conformal. Electronically scanned microstrip arrays make possible an ultra low profile (conformal), low cost design for phased arrays. It may be possible to entirely cover the outer surface of a missile or aircraft with these antennas without large cost or weight penalties.

## Acknowledgment

The author wishes to thank G. Sanford for his support and advice in the preparation of this paper, and M. Perdue for her assistance in editing and typing.

## References

[1] A. Waterman and D. Henry, "Stripline strap-on antenna array," presented at the 21st USAF Antenna Symp.
[2] F. G. Campbell, "An extremely thin omnidirectional microwave antenna array for spacecraft applications," NASA Tech. Note D-5539, Nov. 1969.
[3] H. P. Johnson, "An extremely thin flush mounted slotted linear array," presented at the 16th USAF Antenna Symp.
[4] R. F. Harrington, *Time Harmonic Electromagnetic Fields*. New York: McGraw-Hill, p. 276.
[5] Jasik, *Antenna Engineering Handbook*, p. 3125.
[6] S. Silver, *Microwave Antenna Theory and Design* (M.I.T. Rad. Lab. Series, vol. 12). New York: McGraw-Hill, 1949, p. 178.